IEEE Open Journal of Vehicular Technology

Received 29 March 2024; accepted 3 May 2024. Date of publication 8 May 2024;
date of current version 29 May 2024. The review of this article was coordinated by Editor Xiaoli Chu.

Digital Object Identifier 10.1109/OJVT.2024.3398566

Inter-User Interference Cancellation Scheme for 5G-Based Dynamic Full-Duplex Cellular System

SHOTA MORI (Member, IEEE), KEIICHI MIZUTANI (Member, IEEE), AND HIROSHI HARADA (Senior Member, IEEE)

Graduate School of Informatics, Kyoto University, Kyoto 606-8501, Japan

CORRESPONDING AUTHOR: HIROSHI HARADA (e-mail: hiroshi.harada@i.kyoto-u.ac.jp).

This work was supported in part by the Grant-in-Aid for JSPS Fellows under Grant JP23KJ1330 and in part by the Ministry of Internal Affairs and Communications in Japan under Grant JPJ000254.

ABSTRACT Improving spectral efficiency is an important issue for the next generation of the 5th generation mobile communication (5G) systems. Full-duplex cellular (FDC) and dynamic-FDC (DDC) systems based on the 5G signal format (5G-FDC and 5G-DDC) have gained substantial attention for introducing in-band full-duplex (IBFD) into 5G. However, self-interference (SI) at a base station (BS) and inter-user interference (IUI) in user equipment (UE) are significant hurdles in implementing FDC and DDC systems. This study proposes an IUI cancellation (IUIC) scheme based on successive interference cancellation tailored to the signal configuration and channel coding of 5G. Additionally, we introduce user scheduling and adaptive modulation algorithms for 5G-DDC. We evaluate the proposed schemes using link- and system-level simulations. The results demonstrate a remarkable 40 dB reduction in IUI with a 3.4 dB decline in reception quality. Furthermore, our IUIC method reduces the IUI of close-distance UE pairs, expands the candidate UE pairs for IBFD operation, and significantly enhances the IBFD application ratio in the downlink slot by 51.0% compared to conventional 5G-DDC. Moreover, the gain of the uplink average throughput increases by 11.4% when the BS and UE transmission powers are at their maximum.

INDEX TERMS Dynamic full-duplex cellular, full-duplex cellular, in-band full-duplex, inter-user interference, 5G.

I. INTRODUCTION

Mobile traffic has rapidly surged since the inception of mobile communication systems. In 2020, the 5th generation mobile communication (5G) system was launched to address the increasing demand by leveraging new technologies, such as 5G new radio (NR) and massive multiple-input multiple-output (MIMO) [1]. However, the upsurge in mobile traffic is poised to continue due to advanced use cases encompassing automobiles, telemedicine, and factory automation. Projections suggest that by 2030, approximately 500 billion devices will be interconnected within networks, with machines such as robots, drones, and sensors emerging as the predominant users of mobile communication [2]. Therefore, various technologies have been investigated to improve spectral efficiency and accommodate these burgeoning requirements.

As we move toward the evolution beyond 5G system (5G-Advanced), a spectrum of new technologies, such as sidelink user equipment (UE)-to-UE relay [3], artificial intelligence/machine learning [4], and sub-band non-overlapping full-duplex (SBFD) [5] have been developed within the third-generation partnership project (3GPP) as part of Release 18 [6], [7]. SBFD enables concurrent uplink (UL) and downlink (DL) communication within a shared carrier while judiciously allocating distinct frequency resources to UL and DL communications to prevent interference. SBFD has been verified to improve UL throughput and latency by increasing UL transmission opportunities [5]. However, the DL throughput and latency deteriorate because SBFD does not inherently improve spectral efficiency. SBFD is recognized as an intermediate step, paving the way for the integration of an in-band

full-duplex (IBFD) in the 5G-Advanced evolution or the forthcoming 6th generation mobile communication (6G) system [5], [8]. Hence, the ongoing development of IBFD and SBFD remains imperative.

IBFD is a duplex scheme that enables the simultaneous transmission and reception of signals using the same frequency resources [9], [10], [11], [12], [13], [14], [15], [16], [17], [18], [19], [20], [21], [22], [23], [24], [25]. Ideally, IBFD doubles the spectral efficiency of conventional half-duplex (HD) and SBFD systems. The forthcoming introduction of a full-duplex cellular (FDC) system, embracing IBFD, is anticipated in 5G-Advanved evolution or the advent of 6G. However, IBFD introduces additional interference, such as self-interference (SI) and inter-user interference (IUI). SI arises at the base station (BS), where the DL signal transmitted by the BS substantially degrades the reception quality of the UL signal owing to the proximity of the transmission and reception antennas. Therefore, many studies have proposed passive suppression schemes within the propagation domain and active cancellation schemes within the analog and digital domains [10], [11], [12], [13]. For instance, the SI cancellation performance of wireless fidelity (Wi-Fi) systems can reach up to 110 dB [10]. Digital SI cancellation schemes have been proposed for 5G (referred to as 5G-based SI cancellation) and long-term evolution (LTE) signals in [12] and [13], respectively, significantly enhancing the feasibility of FDC systems.

Conversely, IUI occurs at the UE receiving the DL signal (DL-UE), where the UL signal transmitted by the UE transmitting the UL signal (UL-UE) degrades the reception quality of the DL signal. Various studies have proposed IUI reduction techniques at the physical (PHY) layer [15], [16], [17], [18], [19], [20] and methods for avoiding IUI at the media access control (MAC) layer [21], [22], [23], [24]. In the PHY layer, examples of IUI suppression involve beamforming [15], nulling signal generation and forwarding at the BS [16], [17], polarization state utilization [18], and successive interference cancellation (SIC) [19], [20]. In contrast, IUI avoidance is achieved at the MAC layer by judiciously determining DL-UE and UL-UE pairs that are less susceptible to IUI based on collected IUI information. This approach relies on the propagation loss between UEs and is commonly preferred in IBFD studies owing to its simplicity, resulting in reduced UE circuit complexity and power consumption [21], [22], [23], [24], [25].

A dynamic full-duplex cellular (DDC) system can operate in an environment where some UEs have no function for IBFD operation and represents a pragmatic and incremental approach to FDC implementation employing the MAC layer method [20], [21], [22]. The DDC system operates based on the conventional HD system and activates IBFD when conventional communication in an HD system experiences less degradation owing to IBFD, enabling adaptive IBFD within a reasonable situation. Some FDC systems introduce user scheduling algorithms to maximize the sum of UL and DL throughput [26], [27], but there exists a possibility that user fairness may be ignored. The DDC system aims to maintain the communication quality of the conventional HD system and increases the throughput of all UEs without any degradation. However, the limitation of the FDC system using the MAC-layer method is the potential challenge of not always identifying UE pairs that effectively mitigate IUI, which may hinder IBFD adoption. This scenario is more likely to occur in smaller cell sizes owing to shorter distances between UEs and amplified IUI effects. Therefore, a PHY-layer IUI cancellation (IUIC) scheme employing SIC has been proposed for DDC systems [20], increasing the IBFD-applicability ratio. The method can reduce IUI by digital signal processing of UE even if the number of BS and UE antennas is small. It may increase the computational complexity and power consumption of UE but be more flexible for BS and UE sizes than other schemes. Nevertheless, to the best of our knowledge, directly applying SIC-based IUIC to 5G-based FDC (5G-FDC) or 5G-based DDC (5G-DDC) systems presents several unresolved challenges.

- The conventional IUIC scheme neglects the signal configuration and channel coding inherent in 5G systems.
- The IUIC design must be compatible with SI cancellation methods tailored to 5G-FDC and 5G-DDC.
- IUIC utilization should be minimized to decrease computational complexity and power consumption at the UE, but controlling whether to use IUIC from BS is challenging owing to the fluctuating IUI power resulting from fading and shadowing caused by UE mobility and environmental factors.
- New user scheduling and adaptive modulation algorithms considering the IUIC must be developed.

This study proposes an IUIC based on SIC at the PHY layer for UE in the context of 5G-FDC and 5G-DDC systems. This IUIC is designed to mitigate IUI when the IUI signal is moderately stronger than the desired signal based on the principle of SIC using the power difference between the two signals. The DL-UE firstly demodulates the IUI signal and subtracts it from the received signal. Considering the coexistence of IUIC and SI cancellations, the proposed IUIC leverages the configuration of a demodulation reference signal (DMRS), as originally proposed for SI cancellation [12], to estimate the IUI channel. Subsequently, it removes the IUI signal by demodulating and subtracting it from the received signal. However, an IUIC based on SIC may increase power consumption, as mentioned above. Therefore, we propose a method for determining whether to employ IUIC with the DMRS in the received signal. While demodulating both IUI and desired signals, the UE must decode a low-density parity-check (LDPC) code adopted as channel coding in the 5G system. Successful decoding requires calculating the log-likelihood ratio (LLR). We propose an appropriate method for LLR calculation to enhance the demodulation and IUIC performance when using the 5G-compatible signal. Additionally, we introduce new adaptive modulation and user scheduling algorithms at the MAC layer to advance the development of the proposed IUIC-introduced 5G-DDC. The proposed adaptive

modulation method determines the modulation and coding scheme (MCS) for efficient DL and UL communications with the IUIC. The proposed user scheduling algorithms expand the pool of potential DL-UE and UL-UE candidates in UL and DL slots, respectively, resulting in an augmented ratio of the number of times of applying IBFD to all communication opportunities (i.e., IBFD application ratio).

This study offers several key contributions:

- We propose an IUIC method based on SIC, considering the signal format and channel coding specific to the 5G system. The proposed IUIC aligns seamlessly with SI cancellations for 5G systems because it uses the DMRS configuration employed in 5G-based SI cancellations. Moreover, an LLR calculation method is introduced to enhance the accuracy of demodulation and cancellation.
- We propose a decision-making mechanism to judiciously employ IUIC with the received DMRS, preventing unnecessary activation and conserving resources.
- Adaptive modulation and user scheduling algorithms are proposed to introduce IUIC into the 5G-DDC. These algorithms can expand the number of UE candidates for IBFD and the IBFD application ratios.
- We evaluate the performance of the PHY layer using the proposed IUIC through link-level simulations. Furthermore, the performance of the MAC layer is evaluated using a system-level simulation.

The article structure is as follows: Section II explains the principle of the DDC system. Section III proposes the IUIC based on SIC, including the decision method and LLR calculation. Furthermore, the adaptive modulation and user scheduling schemes are also discussed. Section IV evaluates the PHY-layer performances of the proposed IUIC. Section V assesses the MAC-layer performances of the DDC system using the proposed IUIC. Finally, Section VI concludes the article.

II. DDC SYSTEM

This section elucidates the principles of the DDC system. Subsequently, we explore the interference model and the user scheduling scheme of the DDC system. As an initial study, we assumed a single-cell environment for introducing the IBFD to local 5G to verify the effectiveness of the IUIC in an environment unaffected by other interferences, such as inter-cell interference (ICI). Local 5G predominantly functions as a self-contained system in a private space with a single cell.

A. OUTLINE OF DDC SYSTEM

Fig. 1 illustrates examples of resource allocation. Fig. 1(a) and (b) show a time-division duplex (TDD)-based HD system and the DDC system based on the TDD-based HD system. In this study, one UE or BS or both occupied the available bandwidth. Specifically, frequency-division duplex (FDD) was not considered. Furthermore, this study assumed that UL and DL communications could be switched in each slot (i.e., 14 consecutive orthogonal frequency-division multiplexing (OFDM) symbols).

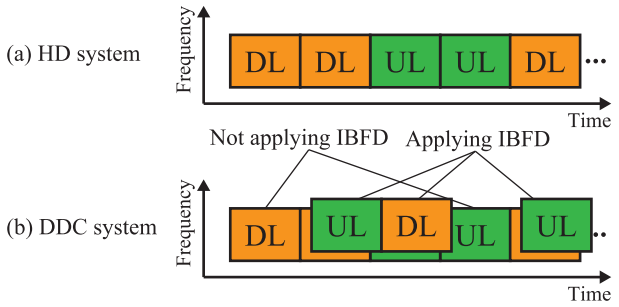

FIGURE 1. Examples of resource allocation.

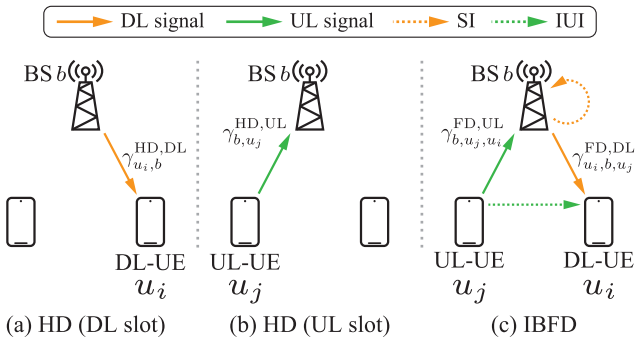

FIGURE 2. Interference model of HD and DDC system.

Fig. 1(a) illustrates that conventional TDD-based HD systems execute UL and DL communications independently. However, the DDC system can fully superimpose DL and UL communications onto the UL and DL slots, respectively, in both the time and frequency resources (Fig. 1(b)). However, the SI and IUI generated by superimposed DL and UL signals, respectively, may degrade their reception quality. Therefore, the DDC system performs IBFD only under the following conditions. The SI must not deteriorate UL communication in the UL slot. However, the IUI must not deteriorate DL communication in a DL slot. A user scheduling scheme was proposed to overcome these limitations and apply IBFD [21], [22].

B. INTERFERENCE MODEL

This section describes the interference model, particularly when implementing IBFD. As mentioned above, the scenario involves a single BS and multiple UEs in a single-cell environment.

1) IN HD OPERATION

In the DL slot (Fig. 2(a)), the received signal-to-noise power ratio (SNR) for DL communication from BS, b, to i-th UE, u_i, is expressed as follows:

$$\gamma^{\mathrm{HD,DL}}_{u_i,b} = \frac{P_b G_{u_i,b} L_{u_i,b} G_{b,u_i}}{N_{u_i} B}, \tag{1}$$

where N_x corresponds to the noise power spectral density of x, B denotes the allocated bandwidth, P_x represents the

transmission power of x, $G_{x,y}$ is the antenna gain of y toward x, and $L_{x,y}$ denotes the path loss between x and y.

In the UL slot (Fig. 2(b)), the received SNR for the UL communication from the j-th UE, u_j, to b is expressed as follows:

$$\gamma_{b,u_j}^{\mathrm{HD,UL}} = \frac{P_{u_j} G_{b,u_j} L_{b,u_j} G_{u_j,b}}{N_b B}. \tag{2}$$

2) IN FD OPERATION

In the IBFD operation (Fig. 2(c)), the received DL and UL signals are affected by IUI and SI, respectively. Therefore, when u_i and u_j denote the DL-UE and UL-UE, respectively, the received signal-to-interference plus noise power ratio (SINR) for the DL and UL communications at u_i and b, respectively, can be expressed as follows:

$$\gamma_{u_i,b,u_j}^{\mathrm{FD,DL}} = \frac{P_b G_{u_i,b} L_{u_i,b} G_{b,u_i}}{N_{u_i} B + P_{u_j} G_{u_i,u_j} L_{u_i,u_j} G_{u_j,u_i}}, \tag{3}$$

$$\gamma_{b,u_j,u_i}^{\mathrm{FD,UL}} = \frac{P_{u_j} G_{b,u_j} L_{b,u_j} G_{u_j,b}}{N_b B + P_b C_{\mathrm{SI}}}, \tag{4}$$

where $C_{\mathrm{SI}} \in [0, 1]$ corresponds to the amount of SI cancellation implemented in the BS.

C. USER SCHEDULING

1) BASIC SCHEDULING METHOD

In 4G and 5G systems, the proportional fairness scheduling (PFS) algorithm is commonly employed [28], [29]. The conventional DDC system also adopted a PFS-based algorithm [21], [22]. The UE allocated for UL communication in the n-th transmission time interval (TTI), $u^{\mathrm{UL}}(n)$, is determined as follows:

$$u^{\mathrm{UL}}(n) = \underset{u_i \in \mathfrak{u}}{\operatorname{argmax}} \frac{R_{u_i}^{\mathrm{UL}}(n)}{\bar{R}_{u_i}^{\mathrm{UL}}(n-1)}, \tag{5}$$

where $R_{u_i}^{\mathrm{UL}}(n)$ and $\bar{R}_{u_i}^{\mathrm{UL}}(n)$ denote the instantaneous UL throughput and exponentially moving averaged UL throughput of u_i at the n-th TTI, respectively. Furthermore, $\mathfrak{u}$ corresponds to the set of potential candidates for the UL-UE who wish to engage in UL communication. The exponentially moving averaged UL throughput is updated for each TTI as follows:

$$\bar{R}_{u_i}^{\mathrm{UL}}(n) = \left(1 - \frac{1}{T_w}\right) \bar{R}_{u_i}^{\mathrm{UL}}(n-1) + \frac{1}{T_w} R_{u_i}^{\mathrm{UL}}(n)\, p_{u_i}^{\mathrm{UL}}(n), \tag{6}$$

where T_w denotes a weighting coefficient and $p_{u_i}^{\mathrm{UL}}(n)$ represents a function that returns 1 when u_i is allocated to UL communication in the n-th TTI; otherwise, it returns 0.

The UE allocated for DL communication, $u^{\mathrm{DL}}(n)$, is determined as follows:

$$u^{\mathrm{DL}}(n) = \underset{u_i \in \mathfrak{D}}{\operatorname{argmax}} \frac{R_{u_i}^{\mathrm{DL}}(n)}{\bar{R}_{u_i}^{\mathrm{DL}}(n-1)}, \tag{7}$$

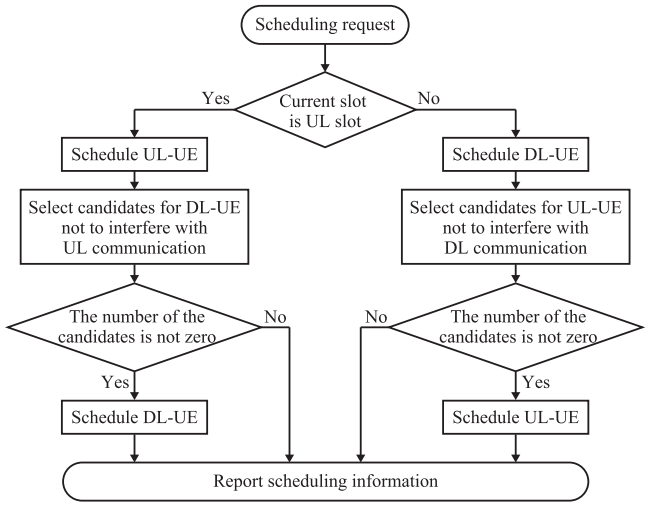

FIGURE 3. Scheduling flow of the conventional DDC system.

$$\bar{R}_{u_i}^{\mathrm{DL}}(n) = \left(1 - \frac{1}{T_w}\right) \bar{R}_{u_i}^{\mathrm{DL}}(n-1) + \frac{1}{T_w} R_{u_i}^{\mathrm{DL}}(n)\, p_{u_i}^{\mathrm{DL}}(n), \tag{8}$$

where $\mathfrak{D}$ corresponds to the set of candidates for the DL-UE that are required to engage in DL communication.

2) DETERMINATION OF IBFD APPLICATION

The DDC system employs a decision-making process to determine whether IBFD should be applied to maintain the reception quality of UL and DL communications in the respective UL and DL slots. Fig. 3 shows the scheduling flow. IBFD can be employed if the MCS used for UL/DL communication in the UL/DL slot remains suitable when superimposed with DL/UL signals (i.e., SI and IUI signals).

In the UL slot, UL-UE u^{UL} is first determined using the PFS algorithm from $\mathfrak{u}$. Subsequently, the DL-UE is selected from the set of potential DL-UE candidates, $\mathfrak{D}^{\mathrm{FD}}$, using the PFS algorithm. $\mathfrak{D}^{\mathrm{FD}}$ is expressed as follows:

$$\mathfrak{D}^{\mathrm{FD}} = \left\{ u_i \in \mathfrak{D} | \omega_{u^{\mathrm{UL}}}^{\mathrm{HD,UL}} = \omega_{u^{\mathrm{UL}},u_i}^{\mathrm{FD,UL}} \wedge \omega_{u_i,u^{\mathrm{UL}}}^{\mathrm{FD,DL}} \neq 0 \right\}, \tag{9}$$

where $\omega_x^{\mathrm{HD,UL}}$ represents the channel quality indicator (CQI) used for UL communication from x to the BS in HD operation, $\omega_{x,y}^{\mathrm{FD,UL}}$ is the CQI from x in FD operation when y is allocated to DL-UE, and $\omega_{x,y}^{\mathrm{FD,DL}}$ is the CQI to x in FD operation when y is allocated to UL-UE. Here, although the CQI is a parameter of the channel state information (CSI) for DL channel in general, the concept of the CQI is also applied to the UL channel in this study. A CQI of zero indicates poor communication conditions, and communication cannot be performed. An adaptive modulation algorithm sets the MCS based on CQI; a function $\psi[\cdot]$ is used to return the maximum CQI to achieve the required block error ratio (BLER) based on the SNR or SINR. CQIs in (9) are determined as follows: $\omega_{u^{\mathrm{UL}}}^{\mathrm{HD,UL}} = \psi[\gamma_{b,u^{\mathrm{UL}}}^{\mathrm{HD,UL}}]$, $\omega_{u^{\mathrm{UL}},u_i}^{\mathrm{FD,UL}} = \psi[\gamma_{b,u^{\mathrm{UL}},u_i}^{\mathrm{FD,UL}}]$, and $\omega_{u_i,u^{\mathrm{UL}}}^{\mathrm{FD,DL}} =$

$\psi[\gamma^{\mathrm{FD,DL}}_{u_i,b,u^{\mathrm{UL}}}]$. If $\mathfrak{D}^{\mathrm{FD}} = \emptyset$, IBFD is not applied. Otherwise, the DL-UE u^{DL} is determined from $\mathfrak{D}^{\mathrm{FD}}$ using the PFS algorithm (see (7)). As shown in (4) and (3), the first and second conditions of (9) are related to SI and IUI, respectively. Hence, the size of $\mathfrak{D}^{\mathrm{FD}}$ is based on the SI cancellation performance and the strength of the IUI. In particular, if the DL-UE lacks an IUIC scheme, it must be positioned far from the UL-UE to decrease the impact of IUI.

In the DL slot, DL-UE u^{DL} is first determined using the PFS algorithm from $\mathfrak{D}$. Subsequently, UL-UE, u^{UL}, is selected from the set of candidates for UL-UE, $\mathfrak{u}^{\mathrm{FD}}$, using the PFS algorithm. $\mathfrak{u}^{\mathrm{FD}}$ is expressed as follows:

$$\mathfrak{u}^{\mathrm{FD}} = \left\{ u_i \in \mathfrak{u} | \omega^{\mathrm{HD,DL}}_{u^{\mathrm{DL}}} = \omega^{\mathrm{FD,DL}}_{u^{\mathrm{DL}},u_i} \wedge \omega^{\mathrm{FD,UL}}_{u_i,u^{\mathrm{DL}}} \neq 0 \right\}, \quad (10)$$

where $\omega^{\mathrm{HD,DL}}_{x}$ represents the CQI for DL communication from the BS to x in HD operation. Therefore, these CQIs are determined as $\omega^{\mathrm{HD,DL}}_{u^{\mathrm{DL}}} = \psi[\gamma^{\mathrm{HD,DL}}_{u^{\mathrm{DL}},b}]$, $\omega^{\mathrm{FD,DL}}_{u^{\mathrm{DL}},u_i} = \psi[\gamma^{\mathrm{FD,DL}}_{u^{\mathrm{DL}},b,u_i}]$, and $\omega^{\mathrm{FD,UL}}_{u_i,u^{\mathrm{DL}}} = \psi[\gamma^{\mathrm{FD,UL}}_{b,u_i,u^{\mathrm{DL}}}]$. If $\mathfrak{u}^{\mathrm{FD}} = \emptyset$, IBFD is not employed. Otherwise, the UL-UE u^{UL} is selected from $\mathfrak{u}^{\mathrm{FD}}$ using the PFS algorithm. Similar to the UL slot, SI and IUI decrease the number of $\mathfrak{u}^{\mathrm{FD}}$.

D. TRANSMISSION POWER CONTROL

In a mobile communication system, the transmission power of the UL-UE should be adjusted based on the path loss between the BS and UL-UE and other parameters to suppress inter-cell interference and UE power consumption. In 5G systems, the transmission power of UE u_i is determined as follows [30]:

$$P_{u_i} = \min\left\{ P^{\max}_{u_i}, P_0 + 10\log_{10}\left(2^{\mu} M\right) + \alpha \Gamma_{u_i,b} \right\}, \quad (11)$$

where $P^{\max}_{u_i}$ corresponds to the maximum transmission power of u_i, P_0 denotes the pre-configured target received power per one RB when the subcarrier spacing, Δf, is 15 kHz, μ corresponds to the numerology determining subcarrier spacing as $\Delta f = 15 \times 2^{\mu}$ kHz [31], M denotes the number of allocated RB for UL communication, $\alpha \in [0, 1]$ is a constant that determines the amount of path loss compensation, and $\Gamma_{u_i,b}$ denotes the path loss between BS b and UE u_i. The received SNR or SINR at BS and reception quality of UL communication increase with α. However, it may also intensify ICI in multicell environments. In our study, α was fixed to one because we only assumed a single-cell environment.

In 5G, the transmission power of the BS is not dynamically adjusted based on the path loss between the BS and the DL-UE. On the other hand, the conventional studies of DDC systems [21], [22] adjusted it based on whether the current slot is a DL or UL slot. In particular, reducing the transmission power of the BS in the UL slot mitigates the impact of SI on desired UL communication and facilitates the DL signal superposition (i.e., realization of IBFD). However, because this assumption was deemed unrealistic and does not satisfy the current 5G standard, the transmission power of the BS was fixed in this study.

III. PROPOSED IUI CANCELLATION METHOD

This section discusses an IUIC scheme suitable for 5G-FDC and 5G-DDC, a method for calculating the LLR when using the proposed IUIC, and a method for determining whether the IUIC should be employed. Additionally, a novel scheduling algorithm and an adaptive modulation scheme are proposed to integrate the IUIC into the 5G-DDC system.

A. PRINCIPLE OF PROPOSED IUI CANCELLATION

Fig. 4 shows a block diagram of the proposed IUIC scheme introduced and implemented within UE. The quantization noise produced by the digital-to-analog converter (DAC) and analog-to-digital converter (ADC) and the nonlinearities of a power amplifier (PA) and a low-noise amplifier (LNA) are not considered. This assumption aligns with common practices in IUIC studies [16], [17], [18]. When operating in IBFD mode, the received signal of the DL-UE in frequency domain, Y, can be expressed as follows:

$$Y = H^{\mathrm{DL}} X^{\mathrm{DL}} + H^{\mathrm{IUI}} X^{\mathrm{UL}} + N, \quad (12)$$

where X^{DL} and X^{UL} denote the transmitted DL and UL signals, respectively. H^{DL} and H^{IUI} represent the DL and IUI channels, respectively. N corresponds to additive white Gaussian noise (AWGN). Uppercase letters indicate variables in the frequency domain.

The DL-UE should eliminate the IUI signal component, $H^{\mathrm{IUI}} X^{\mathrm{UL}}$, but it lacks knowledge of H^{IUI} and X^{UL}. Therefore, similar to [19] and [20], we introduced an IUI cancellation based on SIC in the DL-UE. First, the DL-UE obtains the estimated value of the IUI channel, $\tilde{H}^{\mathrm{IUI}}$, using some known symbol in the received signal, Y. Second, it performs channel equalization and demodulation using $\tilde{H}^{\mathrm{IUI}}$, ultimately deriving the bit stream of the UL signal. Third, DL-UE applies LDPC coding and modulation to the bit stream, producing an estimated UL transmission signal, $\tilde{X}^{\mathrm{UL}}$. Finally, it creates a signal with reduced IUI, Y', by subtracting the replica signal, $\tilde{H}^{\mathrm{IUI}} \tilde{X}^{\mathrm{UL}}$, from Y. Y' can be expressed as follows:

$$\begin{aligned} Y' &= Y - \tilde{H}^{\mathrm{IUI}} \tilde{X}^{\mathrm{UL}} \\ &= H^{\mathrm{DL}} X^{\mathrm{DL}} + \left(H^{\mathrm{IUI}} X^{\mathrm{UL}} - \tilde{H}^{\mathrm{IUI}} \tilde{X}^{\mathrm{UL}} \right) + N. \end{aligned} \quad (13)$$

Subsequently, the DL-UE demodulates Y' as the DL signal (i.e., the desired signal) and obtains the desired bit stream. When the estimation accuracy of the IUI channel and the demodulation accuracy of the UL signal are sufficiently high (i.e., $H^{\mathrm{IUI}} \approx \tilde{H}^{\mathrm{IUI}}$ and $X^{\mathrm{UL}} \approx \tilde{X}^{\mathrm{UL}}$), the residual IUI signal component, $H^{\mathrm{IUI}} X^{\mathrm{UL}} - \tilde{H}^{\mathrm{IUI}} \tilde{X}^{\mathrm{UL}}$, is negligible. However, if either or both of the factors degrade, the residual IUI signal component will grow, deteriorating the demodulation accuracy of the desired signal. Therefore, it is imperative to improve the estimation accuracy of H^{IUI} and X^{UL}.

To improve the estimation accuracy of $H^{\mathrm{IUI}}$and consequently enhance the efficacy of IUI cancellation, we should use the demodulation reference signal (DMRS) for demodulating PDSCH/PUSCH in the 5G system [31]. However, in the current 5G systems, which do not operate as FDC systems, the UL/DL signals may interfere with the DMRSs contained

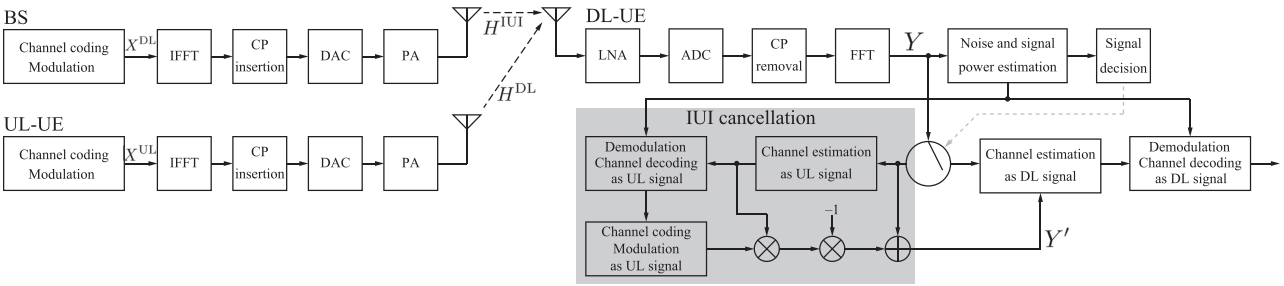

FIGURE 4. Block diagram of the proposed IUI cancellation.

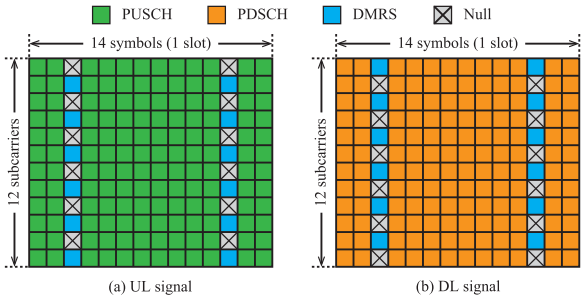

FIGURE 5. Resource allocation examples for the proposed IUI cancellation.

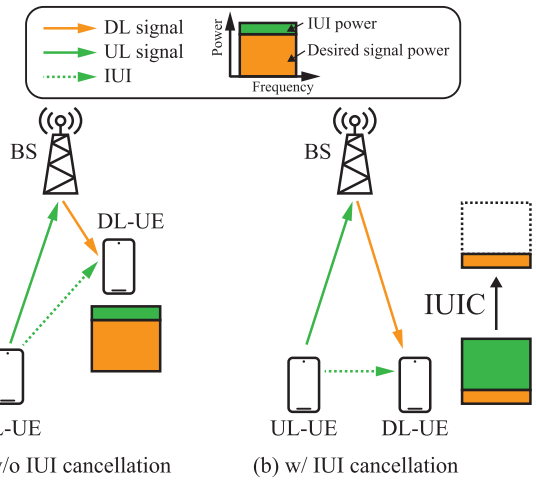

FIGURE 6. Difference of the operation of DL-UE.

in the DL/UL signal (DL-DMRS/UL-DMRS). Hence, we adopted the DMRS configuration proposed for 5G-based SI cancellation [12].

As shown in Fig. 5, the positioning of DL-DMRS and UL-DMRS is designed to minimize interference from other signals. This configuration ensures that $\tilde{H}^{\mathrm{IUI}}$ and $\tilde{H}^{\mathrm{DL}}$ during IBFD are equivalent to those during HD. Additionally, 5G-based SI and IUI cancellations can coexist using the same DMRS configuration as the 5G-based SI cancellation. In 5G, the maximum number of OFDM symbols containing a DMRS in a slot is four (i.e., 14 consecutive OFDM symbols) [31]. We assumed two OFDM symbols with DMRS in a slot.

B. PROPOSED DECISION METHOD FOR THE USE OF IUI CANCELLATION

In this section, we introduce a decision method for using an IUIC based on the received signal. The necessity of IUI cancellation varies based on the radio propagation environment, influenced by the location of the DL-UE, UL-UE, and nearby objects. As depicted in Fig. 6(a), when the propagation loss of the IUI channel is large, and the received DL power at DL-UE is stronger than the IUI power, the DL-UE should directly demodulate the DL signal. However, when the propagation loss of the IUI channel is small, and the DL power is smaller than the IUI power, the DL-UE should demodulate the DL signal after reducing the IUI signal component using the IUIC based on the SIC (Fig. 6(b)).

The BS can regulate whether the DL-UE employs the IUIC based on the previously reported IUI information. Nevertheless, this control information may be erroneous owing to instantaneous fluctuations in the DL and IUI channels. Therefore, we propose a decision method that leverages the characteristics of the DMRS configuration described in Section III-A. The received DL-DMRS, Y^{DLD}, and UL-DMRS, Y^{ULD}, can be expressed as follows because the DL-DMRS and UL-DMRS remain unaffected by the UL and DL signals, respectively:

$$Y^{\mathrm{DLD}} = H^{\mathrm{DL}} X^{\mathrm{DLD}} + N, \tag{14}$$

$$Y^{\mathrm{ULD}} = H^{\mathrm{IUI}} X^{\mathrm{ULD}} + N, \tag{15}$$

where X^{DLD} and X^{ULD} denote the transmitted DL-DMRS and UL-DMRS, respectively. First, the estimated noise power, $\widetilde{\sigma^2}$, is obtained using DL-DMRS, following a procedure similar to 5G-based SI cancellation [12]. Subsequently, the powers of DL-DMRS, P^{DL}, and UL-DMRS, P^{IUI}, are calculated as follows:

$$P^{\mathrm{DL}} = \mathrm{E}\left[\left|Y^{\mathrm{DLD}}\right|^2\right] - \widetilde{\sigma^2}, \tag{16}$$

$$P^{\mathrm{IUI}} = \mathrm{E}\left[\left|Y^{\mathrm{ULD}}\right|^2\right] - \widetilde{\sigma^2}, \tag{17}$$

where $\mathrm{E}[\cdot]$ represents the expected value. Finally, they are used to determine whether the proposed IUIC can be used. If $P^{\mathrm{DL}} > P^{\mathrm{IUI}}$, the DL-UE refrains from employing the IUIC and demodulates the received signal, Y, as the desired signal. However, if $P^{\mathrm{DL}} \leq P^{\mathrm{IUI}}$, the DL-UE proceeds with the IUIC to obtain the residual signal, Y', as the desired signal.

C. PROPOSED LLR CALCULATION METHOD

The demodulation accuracy of the IUI signal must be sufficiently high to enhance the performance of the IUIC. In 5G systems, binary LDPC code is employed as an error correction code for the PHY DL/UL shared channel (PDSCH/PUSCH), which is used for user data transmission [32]. LDPC is defined by an extremely sparse parity-check matrix and offers high error correction performance, particularly when the code is sufficiently long, approaching the Shannon limit asymptotically. The input to the decoder is the LLR of the received signal. The accuracy of the LLR calculation significantly affects the decoding performance.

The LLR of the j-th bit in the i-th received signal, $\lambda_{i,j}$, is defined as

$$\lambda_{i,j} = \log \frac{P\left(y_i | x_{i,j} = 0\right)}{P\left(y_i | x_{i,j} = 1\right)}, \tag{18}$$

where y_i denotes the i-th received symbol, and $x_{i,j}$ represents the j-th bit in the i-th transmitted symbol. In the AWGN channel, $\lambda_{i,j}$ is calculated as follows:

$$\lambda_{i,j} = \log \frac{\sum_{s \in S_0} \exp\left[-\frac{1}{\sigma^2}\left\{\left(y_{i,x} - s_x\right)^2 + \left(y_{i,y} - s_y\right)^2\right\}\right]}{\sum_{s \in S_1} \exp\left[-\frac{1}{\sigma^2}\left\{\left(y_{i,x} - s_x\right)^2 + \left(y_{i,y} - s_y\right)^2\right\}\right]}, \tag{19}$$

where S_0 and S_1 denote the sets of ideal constellation points with j-th bits equal to 0 and 1, respectively. Furthermore, s_x and s_y correspond to the in-phase and quadrature coordinates of S_0 and S_1, respectively; $y_{i,x}$ and $y_{i,y}$ represent the in-phase and quadrature coordinates of y_i, respectively. Moreover, σ^2 denotes the power of AWGN. In the case of a fading channel, the LLR can be calculated according to (19) after equalizing the channel.

However, as shown in (19), the computational complexity increases exponentially with higher modulation levels. Therefore, LLR can be approximately calculated using the terms that express the closest points in S_0 and S_1 to the received symbol, as follows [33]:

$$\begin{aligned}\lambda_{i,j} = -\frac{1}{\sigma^2}\Bigg[&\min_{s \in S_0}\left\{\left(y_{i,x} - s_x\right)^2 + \left(y_{i,y} - s_y\right)^2\right\} \\ &- \min_{s \in S_1}\left\{\left(y_{i,x} - s_x\right)^2 + \left(y_{i,y} - s_y\right)^2\right\}\Bigg].\end{aligned} \tag{20}$$

In this study, we calculated the LLR according to (19) for the QPSK symbols and (20) for the 16QAM and 64QAM symbols.

As mentioned earlier, the accuracy of LLR calculation plays a pivotal role in demodulating 5G signals. Therefore, an LLR calculation method considering the IBFD operation must be adopted. Therefore, it is proposed for all cases irrespective of whether the IUIC is applied.

1) WHEN NOT USING THE IUI CANCELLATION

The received signal is demodulated directly as the desired signal when the IUIC is not used; however, an IUI signal component exists. Therefore, the noise power terms in (19) and (20) are replaced as follows:

$$\sigma^2 = \widetilde{\sigma^2} + P^{\mathrm{IUI}}. \tag{21}$$

The IUI signal is assumed to follow a Gaussian distribution.

2) WHEN USING THE IUI CANCELLATION

LLR calculation involves two stages when the IUIC is employed: one for the IUI signal and the other for the desired signal after IUIC. Therefore, we demodulate the IUI signal, which resulted in the desired DL signal being treated as an interference signal in the initial LLR calculations. Therefore, the noise power terms in (19) and (20) are substituted as follows:

$$\sigma^2 = \widetilde{\sigma^2} + P^{\mathrm{DL}}, \tag{22}$$

where the DL signal is assumed to follow a Gaussian distribution. In the second stage, when the desired signal is demodulated after IUIC, a residual IUI component remains, as shown in (13). In this case, the noise power terms are replaced, as shown in (23). The rationale here is that when the demodulation accuracy of the IUI signal is sufficiently high, IUI and SI cancellations can be considered equivalent. Therefore, only the estimated noise power term is utilized [12]. The noise terms are replaced as follows:

$$\sigma^2 = \widetilde{\sigma^2}. \tag{23}$$

These modifications reflect how the noise terms are adapted when performing LLR calculations in the presence of IUI cancellation in the IUIC scheme. This ensures that the noise power is correctly accounted for during demodulation and reflects the actual interference conditions at each stage of signal processing.

D. PROPOSED USER SCHEDULING AND ADAPTIVE MODULATION ALGORITHMS WITH THE PROPOSED IUI CANCELLATION

In the conventional DDC system, the IUI component is treated as noise. If the IUI power becomes significantly strong, it prevents DL-UE from demodulating the DL signal, hindering the application of IBFD. However, introducing the proposed IUIC enables situations where the IUI power is *moderately stronger* than the DL signal power to still enable the DL-UE to extract and demodulate the desired signal. The proposed new user scheduling and adaptive modulation algorithms are shown in Algorithm 1 and Algorithm 2 for the DL and UL slots, respectively, to control and maximize the effectiveness of the IUIC.

1) IN DL SLOT

In the DL slot, candidates for the UL-UE, $\mathrm{u}_{\mathrm{IUIC}}^{\mathrm{FD}}$, intending the DL-UE to use the IUIC are selected in addition to the conventional DDC system. After determining u^{DL} and u^{FD} following the conventional DDC system procedures, the CQI for UL communication in the DL slot, incorporating the proposed IUIC, $\omega_{u_i,u^{\mathrm{DL}}}^{\mathrm{FD,UL,IUIC}}$, is calculated. $\omega_{u_i,u^{\mathrm{DL}}}^{\mathrm{FD,UL,IUIC}}$ is determined as

Algorithm 1: User Scheduling and Adaptive Modulation Algorithm in DL Slot in the DDC System Using IUI Cancellation.

Estimate $\gamma_{u_i,b}^{\mathrm{HD,DL}}$ and determine $\omega_{u_i}^{\mathrm{HD,DL}} = \psi[\gamma_{u_i,b}^{\mathrm{HD,DL}}]$ for all $u_i \in \mathfrak{D}$
Select one $u^{\mathrm{DL}} = u_i$ from $\mathfrak{D}$ by PFS algorithm
Estimate $\gamma_{u^{\mathrm{DL}},b,u_i}^{\mathrm{FD,DL}}$ and $\gamma_{u_i,b,u^{\mathrm{DL}}}^{\mathrm{FD,UL}}$ and determine $\omega_{u^{\mathrm{DL}},u_i}^{\mathrm{FD,DL}} = \psi[\gamma_{u^{\mathrm{DL}},b,u_i}^{\mathrm{FD,DL}}]$ and $\omega_{u_i,u^{\mathrm{DL}}}^{\mathrm{FD,UL}} = \psi[\gamma_{b,u_i,u^{\mathrm{DL}}}^{\mathrm{FD,UL}}]$ for all $u_i \in \mathfrak{u}$
Select candidates for UL-UE intending DL-UE not to use the IUIC as $\mathfrak{u}^{\mathrm{FD}} = \{u_i \in \mathfrak{u} | \omega_{u^{\mathrm{DL}}}^{\mathrm{HD,DL}} = \omega_{u^{\mathrm{DL}},u_i}^{\mathrm{FD,DL}} \wedge \omega_{u_i,u^{\mathrm{DL}}}^{\mathrm{FD,UL}} \neq 0\}$
Estimate $\varepsilon_{u^{\mathrm{DL}},b,u_i}^{\mathrm{FD,DL}}$ and $\delta_{u^{\mathrm{DL}},b,u_i}^{\mathrm{FD,DL}}$ and determine $\omega_{u_i,u^{\mathrm{DL}}}^{\mathrm{FD,UL,IUIC}} = \min(\omega_{u_i,u^{\mathrm{DL}}}^{\mathrm{FD,UL}}, \psi[\varepsilon_{u^{\mathrm{DL}},b,u_i}^{\mathrm{FD,DL}}])$ for all $u_i \in \mathfrak{u}$
Select candidates for UL-UE intending DL-UE to use the IUIC as $\mathfrak{u}_{\mathrm{IUIC}}^{\mathrm{FD}} = \{u_i \in \mathfrak{u} | \omega_{u_i,u^{\mathrm{DL}}}^{\mathrm{FD,UL,IUIC}} \neq 0 \wedge \delta_{u^{\mathrm{DL}},b,u_i}^{\mathrm{FD,DL}} > \rho\}$
If $\{\mathfrak{u}^{\mathrm{FD}} \cup \mathfrak{u}_{\mathrm{IUIC}}^{\mathrm{FD}}\}$ is not empty set **then**
    Choose one $u^{\mathrm{UL}} = u_i$ from $\{\mathfrak{u}^{\mathrm{FD}} \cup \mathfrak{u}_{\mathrm{IUIC}}^{\mathrm{FD}}\}$ by PFS algorithm
End If
End Procedure

Algorithm 2: User Scheduling and Adaptive Modulation Algorithm in UL Slot in the DDC System Using IUI Cancellation.

Estimate $\gamma_{b,u_i}^{\mathrm{HD,UL}}$ and determine $\omega_{u_i}^{\mathrm{HD,UL}} = \psi[\gamma_{b,u_i}^{\mathrm{HD,UL}}]$ for all $u_i \in \mathfrak{u}$
Select one $u^{\mathrm{UL}} = u_i$ from $\mathfrak{u}$ by PFS algorithm
Estimate $\gamma_{b,u^{\mathrm{UL}},u_i}^{\mathrm{FD,UL}}$ and $\gamma_{u_i,b,u^{\mathrm{UL}}}^{\mathrm{FD,DL}}$ and determine $\omega_{u^{\mathrm{UL}},u_i}^{\mathrm{FD,UL}} = \psi[\gamma_{b,u^{\mathrm{UL}},u_i}^{\mathrm{FD,UL}}]$ and $\omega_{u_i,u^{\mathrm{UL}}}^{\mathrm{FD,DL}} = \psi[\gamma_{u_i,b,u^{\mathrm{UL}}}^{\mathrm{FD,DL}}]$ for all $u_i \in \mathfrak{D}$
Select candidates for DL-UE intending not to use the IUIC as $\mathfrak{D}^{\mathrm{FD}} = \{u_i \in \mathfrak{D} | \omega_{u^{\mathrm{UL}}}^{\mathrm{HD,UL}} = \omega_{u^{\mathrm{UL}},u_i}^{\mathrm{FD,UL}} \wedge \omega_{u_i,u^{\mathrm{UL}}}^{\mathrm{FD,DL}} \neq 0\}$
Estimate $\gamma'^{\mathrm{FD,DL}}_{u_i,b,u^{\mathrm{UL}}}$ and determine $\omega_{u_i,u^{\mathrm{UL}}}^{\mathrm{FD,DL,IUIC}} = \psi[\gamma'^{\mathrm{FD,DL}}_{u_i,b,u^{\mathrm{UL}}}]$ for all $u_i \in \mathfrak{D}$
Select candidates for UL-UE intending to use the IUIC as $\mathfrak{D}_{\mathrm{IUIC}}^{\mathrm{FD}} = \{u_i \in \mathfrak{D} | \omega_{u_i,u^{\mathrm{UL}}}^{\mathrm{FD,DL,IUIC}} \neq 0 \wedge \delta_{u_i,b,u^{\mathrm{UL}}}^{\mathrm{FD,DL}} > \rho \wedge \varepsilon_{u_i,b,u^{\mathrm{UL}}}^{\mathrm{FD,DL}} > \theta \wedge \omega_{u^{\mathrm{UL}}}^{\mathrm{HD,UL}} = \omega_{u^{\mathrm{UL}},u_i}^{\mathrm{FD,UL}}\}$
If $\{\mathfrak{D}^{\mathrm{FD}} \cup \mathfrak{D}_{\mathrm{IUIC}}^{\mathrm{FD}}\}$ is not empty set **then**
    Choose one $u^{\mathrm{DL}} = u_i$ from $\{\mathfrak{D}^{\mathrm{FD}} \cup \mathfrak{D}_{\mathrm{IUIC}}^{\mathrm{FD}}\}$ by PFS algorithm
End If
End Procedure

follows because the UL signal must be demodulated at not only BS but also DL-UE to ensure high estimation accuracy of $\tilde{X}^{\mathrm{UL}}$:

$$\omega_{u_i,u^{\mathrm{DL}}}^{\mathrm{FD,UL,IUIC}} = \min\left(\omega_{u_i,u^{\mathrm{DL}}}^{\mathrm{FD,UL}}, \psi\left[\varepsilon_{u^{\mathrm{DL}},b,u_i}^{\mathrm{FD,DL}}\right]\right), \tag{24}$$

where $\varepsilon_{u^{\mathrm{DL}},b,u_i}^{\mathrm{FD,DL}}$ signifies the interference-to-signal plus noise ratio (ISNR) at DL-UE. When u_i and u_j denote the DL-UE and UL-UE, respectively, $\varepsilon_{u_i,b,u_j}^{\mathrm{FD,DL}}$ is calculated as follows:

$$\varepsilon_{u_i,b,u_j}^{\mathrm{FD,DL}} = \frac{P_{u_j} G_{u_i,u_j} L_{u_i,u_j} G_{u_j,u_i}}{N_{u_i} B + P_b G_{u_i,b} L_{u_i,b} G_{b,u_i}}. \tag{25}$$

Subsequently, $\mathfrak{u}_{\mathrm{IUIC}}^{\mathrm{FD}}$ is selected. The first condition to ensure the value of UL communication is $\omega_{u_i,u^{\mathrm{DL}}}^{\mathrm{FD,UL,IUIC}} \neq 0$. This condition aligns with the one used for the selection of $\mathfrak{u}^{\mathrm{FD}}$. The second condition is $\delta_{u^{\mathrm{DL}},b,u_i}^{\mathrm{FD,DL}} > \rho$, which ensures that the IUI power is not excessively large to surpass the IUIC performance. Here, $\delta_{u^{\mathrm{DL}},b,u_i}^{\mathrm{FD,DL}}$ and ρ denote the signal-to-interference power ratio (SIR) at DL-UE u^{DL} and the SIR threshold, respectively. When u_i and u_j denote the DL-UE and UL-UE, respectively, $\delta_{u_i,b,u_j}^{\mathrm{FD,DL}}$ is calculated as follows:

$$\delta_{u_i,b,u_j}^{\mathrm{FD,DL}} = \frac{P_b G_{u_i,b} L_{u_i,b} G_{b,u_i}}{P_{u_j} G_{u_i,u_j} L_{u_i,u_j} G_{u_j,u_i}}. \tag{26}$$

Note that ρ should be adjusted properly based on the result of the link-level simulation of the proposed IUIC.

Subsequently, u^{UL} is selected from the union of sets $\mathfrak{u}^{\mathrm{FD}}$ and $\mathfrak{u}_{\mathrm{IUIC}}^{\mathrm{FD}}$ using the PFS algorithm. Therefore, introducing the proposed IUIC can increase the range of UL-UE selections.

2) IN UL SLOT

In the UL slot, similar to the DL slot, candidates for DL-UE, $\mathfrak{D}_{\mathrm{IUIC}}^{\mathrm{FD}}$, are selected, aiming to use the IUIC. After determining u^{UL} and $\mathfrak{D}^{\mathrm{FD}}$ following the conventional DDC system procedures, the algorithm calculates the CQI for DL communication in the UL slot with the proposed IUIC, $\omega_{u_i,u^{\mathrm{UL}}}^{\mathrm{FD,DL,IUIC}}$. The residual IUI power should be considered when deciding on its value. However, accurate estimation of the strength of the residual IUI power is challenging because it depends on the estimation accuracies of $\tilde{H}^{\mathrm{IUI}}$ and $\tilde{X}^{\mathrm{UL}}$ (13). Therefore, $\omega_{u_i,u^{\mathrm{UL}}}^{\mathrm{FD,DL,IUIC}}$ is determined based on the potential SINR at DL-UE after processing the IUIC, $\gamma'^{\mathrm{FD,DL}}_{u_i,b,u^{\mathrm{UL}}}$, which is estimated as follows:

$$\gamma'^{\mathrm{FD,DL}}_{u_i,b,u^{\mathrm{UL}}} = \frac{P_b G_{u_i,b} L_{u_i,b} G_{b,u_i}}{N_{u_i} B + P_{u^{\mathrm{UL}}} G_{u_i,u^{\mathrm{UL}}} L_{u_i,u^{\mathrm{UL}}} G_{u^{\mathrm{UL}},u_i} C_{\mathrm{IUI}}}, \tag{27}$$

where $C_{\mathrm{IUI}} \in [0, 1]$ indicates the potential cancellation amount of the proposed IUIC implemented in the UE.

Subsequently, $\mathfrak{D}_{\mathrm{IUIC}}^{\mathrm{FD}}$ is selected. The first and second conditions are approximately identical to those in the DL slot. Additionally, the third condition of $\varepsilon_{u_i,b,u^{\mathrm{UL}}}^{\mathrm{FD,DL}} > \theta$ ensures that DL-UE can demodulate the IUI signal for the IUIC using SIC. θ denotes the SINR threshold, which can achieve the

TABLE 1. Link-Level Simulation Parameters

Parameter	Value
Channel bandwidth	40 MHz
Subcarrier spacing	30 kHz
Allocated bandwidth	106 PRBs
FFT size	2048
CP rate	144/2048(all symbols)
Sampling rate	30.688 MHz
Coding scheme	NR LDPC
Modulation scheme	64QAM
Code rate	466/1024
Decoding algorithm	Log-domain sum-product
Decoding iteration	50
Carrier frequency	4 GHz
Channel	TDL-A (delay spread: 100 ns) [34]
Moving speed	3 km/h (11.1 Hz)
Antenna	Tx: 1, Rx, 1

required BLER using $\omega_{u^{\mathrm{UL}}}^{\mathrm{HD,UL}}$. This condition is not required in the DL slot because it is inherently satisfied by the proposed adaptive modulation algorithm. Finally, the fourth condition checks if $\omega_{u^{\mathrm{UL}}}^{\mathrm{HD,UL}} = \omega_{u^{\mathrm{UL}},u_i}^{\mathrm{FD,UL}}$, which remains consistent with the conventional DDC system.

Finally, u^{DL} is selected from the union of sets $\mathfrak{D}^{\mathrm{FD}}$ and $\mathfrak{D}_{\mathrm{IUIC}}^{\mathrm{FD}}$ using the PFS algorithm.

IV. LINK-LEVEL EVALUATION OF PROPOSED IUI CANCELLATION

In this section, the performance of the proposed IUIC scheme is evaluated using a link-level simulation.

A. LINK-LEVEL SIMULATION PARAMETERS

Table 1 lists the link-level simulation parameters. The same parameters were used for the DL signal (i.e., the desired signal) and UL signal (i.e., the IUI signal). However, their DMRS configurations differed, as depicted in Fig. 5. The transmission and reception antennas of the BS and UE were assumed to be single-input single-output (SISO). The channel model employed for both the DL and IUI signals was the TDL-A model, as defined by 3GPP [34]. The TDL-A model enables customization of the delay spread, which, in this study, was set to 100 ns, representing the average value in a non-line-of-sight environment. Assuming that the UE and objects around the BS moved at 3 km/h, the maximum Doppler frequencies of the DL and IUI channels were set to 11.1 Hz. In this study, the IUIC performance was evaluated based on the BLER performance of the desired signal. The required BLER was set to 0.1. Additionally, it was assumed that the DL-UE can receive the DL and IUI signal completely simultaneously. The effect caused by the gap in reception timing is left for future study.

B. BLER PERFORMANCE

Figs. 7 and 8 illustrate the BLER performance of the IBFD as a function of SIR when the SNR is fixed at 20 dB. Figs. 7 and 8 present the BLER characteristics under the following two conditions for the noise power terms in the LLR calculation:

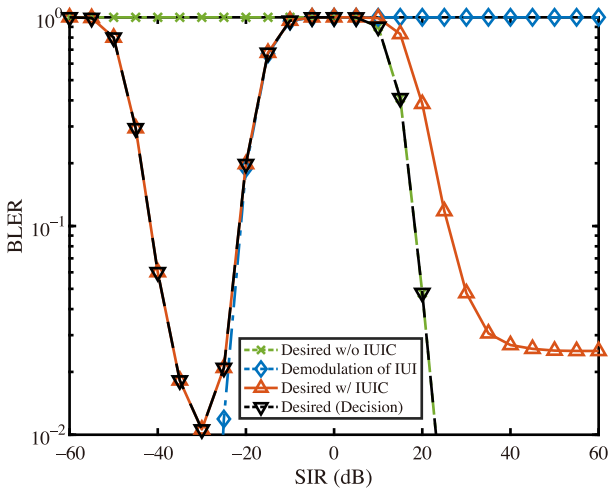

FIGURE 7. BLER characteristics with the proposed IUI cancellation as a function of SIR (Case-1).

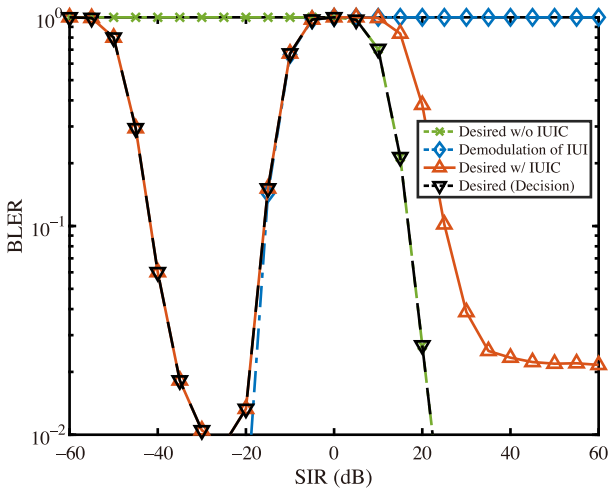

FIGURE 8. BLER characteristics with the proposed IUI cancellation as a function of SIR (Case-2).

Case-1. Only the estimated noise power $\widetilde{\sigma^2}$ is used.

Case-2. The estimated noise power $\widetilde{\sigma^2}$ and signal powers P^{IUI} and P^{DL} are used, following the approach outlined in Section III-C.

The red solid and green dashed lines represent the BLER characteristics with and without the IUIC, respectively. The blue dashed line represents the demodulation accuracy of the IUI signals in IUIC. The black dashed line corresponds to the BLER characteristics when the proposed decision method is introduced.

First, when the IUIC is not employed, Case-1 and Case-2 exhibit nearly identical characteristics. As the SIR increases (i.e., the IUI power decreases), the BLER performance improves. The threshold SIRs required to achieve the target BLER in Case-1 and Case-2 are 18.3 dB and 16.8 dB, respectively. It indicates that the proposed LLR calculation method

increases the maximum allowable power of the IUI signal by 1.5 dB.

Second, the IUI demodulation accuracy improves as the SIR decreases (i.e., the IUI power increases), regardless of the LLR calculation method. However, Case-2 exhibits a steeper decline in BLER than Case-1. In Case-1 and Case-2, the threshold SIR values are -21.2 dB and -15.5 dB, respectively. It implies that the proposed LLR calculation method improves the IUI demodulation accuracy by 5.7 dB, decreasing the residual IUI signal component. Hence, Case-1 and Case-2 can achieve the required BLER using the proposed IUIC in the range of -41.6 dB $<$ SIR $<$ -21.5 dB and -41.6 dB $<$ SIR $<$ -15.9 dB, respectively. This result highlights that the proposed LLR calculation method extends the SIR range in which the required BLER can be achieved using the IUIC by 5.6 dB. In the SIR range where SIR $<$ 0 dB, the upper threshold is determined by the IUI demodulation accuracy. Conversely, the lower threshold of the SIR is determined by decreasing the effective SINR because the residual IUI component primarily arises from the errors in estimating the IUI channel. In this context, even with the IUIC, the required BLER can be achieved when SIR $>$ 0 dB though the IUI power is significantly low to accurately demodulate the IUI signal. This is because the absolute value of the estimated IUI channel, $\tilde{H}^{\mathrm{IUI}}$, becomes small. Hence, when the IUI power is sufficiently small, the received signal after the IUIC can be expressed as $Y' = Y - \tilde{H}^{\mathrm{IUI}}\tilde{X}^{\mathrm{UL}} \approx Y$. However, Fig. 8 shows that the threshold SIR with the IUIC is 8.3 dB higher than that without the IUIC. Therefore, the UE should be equipped with a decision method to reduce the computational complexity and power consumption and maximize the allowable IUI power range.

Third, the BLER characteristics obtained using the proposed decision method in both Case-1 and Case-2 conform to the best BLER characteristics. Therefore, the proposed method can effectively determine whether to employ IUIC based on the received signal and maximize the SIR range to attain the required BLER. In Case-2, the required BLER can be achieved within the range of -41.6 dB $<$ SIR $<$ -15.9 dB or 16.8 dB $<$ SIR.

Finally, Fig. 9 shows the BLER characteristics of IBFD in Case-2 as a function of the SNR under the conditions of SIR at -45 dB, -40 dB, -20 dB, 0 dB, 20 dB, and 40 dB. The BLER characteristics of the HD are illustrated for comparison. The BLER curve for SIR $=$ 40 dB matches with that of the HD because the IUI power is negligibly small. The situation can be considered as HD in the SNR range of $<$ 20 dB. When SIR is -40 dB, -20 dB, and 20 dB, the BLER characteristics decrease as SNR increases. However, they deteriorate compared to the HD because the SINR becomes worse than the SNR and cannot exceed 20 dB, primarily owing to the IUI power when the IUIC is not used under SIR $=$ 20 dB. Conversely, in the case of SIR of -40 dB and -20 dB, where the IUIC is used, the residual IUI signal degrades the effective SINR after the IUIC, even if SNR is improved. When SIR $=$ -45 dB, the required BLER cannot be achieved due to a severe drop in the effective SINR after the IUIC. Finally, when SIR $=$ 0 dB, demodulating the desired signal is impossible owing to the lack of power difference between the desired and IUI signals to directly demodulate the desired signal or use the proposed IUIC based on SIC.

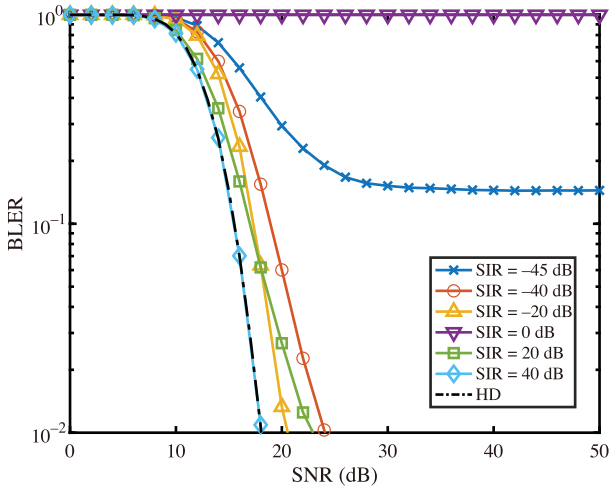

FIGURE 9. BLER characteristics with the proposed IUI cancellation as a function of SNR.

The required SNRs to achieve the required BLER under the condition of HD and SIR of 40 dB, 20 dB, -20 dB, and -40 dB are 15.5 dB, 15.5 dB, 17.0 dB, 17.3 dB, and 18.9 dB, respectively. These values vary with the SIR. Therefore, introducing IUIC may adversely impact the system throughput without well-designed user scheduling and adaptive modulation algorithms.

V. SYSTEM-LEVEL EVALUATION OF DDC SYSTEM APPLYING PROPOSED IUI CANCELLATION

This section discusses the performance of a 5G-DDC system applying the proposed IUIC through a system-level simulation.

A. SYSTEM-LEVEL SIMULATION CONFIGURATION

Table 2 presents the system-level simulation parameters. We evaluated the proposed schemes in a single-cell environment, which can be considered a local 5G scenario. The parameters were determined based on [34] and [35]. The indoor factory (InF)-DH and InF-SL models defined in 3GPP were used for the channel models between the BS and UE and between the UE and UE, respectively. Generally, the InF model is used only for channels between the BS and the UE [34]. However, we applied the InF model to the channel between the UE by setting the heights of the transmission and reception antenna to the same value, following a similar approach as in [36]. The factory hall size was 50 $\times$ 50 m, the room height was set to 10 m, and the BS was fixed at the center of the hall. These are equivalent to one cell extracted from the multi-cell environment for the InF scenario. The ten UE were uniformly

TABLE 2. System-Level Simulation Parameters

Parameter	Value
BS maximum Tx power	27 dBm
BS antenna height	8 m
BS antenna pattern / gain	Omnidirectional / 5 dBi
BS noise figure	5 dB
UE maximum Tx power	23 dBm
UE antenna height	1.5 m
UE antenna pattern / gain	Isotropic / 0 dBi
UE noise figure	9 dB
Thermal noise power	–96 dBm
SI cancellation	110 dB
Channel model (BS–UE)	3GPP, InF-DH [34]
Channel model (UE–UE)	3GPP, InF-SL [34]
Clutter height	2 m
Clutter size	10 m
Clutter density	20%
Shadowing correlation	0
Moving speed	3 km/h
Base duplex scheme	TDD (DL:UL = 5:5)
Traffic model	Full buffer model

TABLE 3. CQI Table and Available SINR Range

CQI	Modulation	Code rate (×1024)	Available SINR range (to fulfill the required BLER of 10^{-1})
0			Less than –0.7 dB
1	QPSK	78	From –0.7 dB to 0.6 dB
2	QPSK	120	From 0.6 dB to 2.3 dB
3	QPSK	193	From 2.3 dB to 4.4 dB
4	QPSK	308	From 4.4 dB to 6.4 dB
5	QPSK	449	From 6.4 dB to 9.6 dB
6	QPSK	602	From 9.6 dB to 10.1 dB
7	16QAM	378	From 10.1 dB to 12.3 dB
8	16QAM	490	From 12.3 dB to 15.3 dB
9	16QAM	616	From 15.3 dB to 16.3 dB
10	64QAM	466	From 16.3 dB to 18.3 dB
11	64QAM	567	From 18.3 dB to 21.2 dB
12	64QAM	666	From 21.2 dB to 24.1 dB
13	64QAM	772	From 24.1 dB to 27.2 dB
14	64QAM	873	From 27.2 dB to 31.0 dB
15	64QAM	948	More than 31.0 dB

distributed randomly on the floor and assumed to move randomly at a 3 km/h speed. The SI cancellation performance was set to 110 dB, as reported in [10].

In the system-level simulation, radio channel realizations were obtained according to stepwise procedures [34]. The BS and UL-UE generated DL and UL signals, respectively, and BS and DL-UE demodulated the UL and DL signals, which included the IUI signal, respectively. Therefore, a link-level simulation was performed for each loop. The parameters for the link-level simulation were consistent with those in Table 1, except for the channel model and moving speed, which were incorporated into the radio channel realizations. The modulation scheme and code rate differed due to the introduction of the proposed adaptive modulation algorithm.

The MCS used for UL or DL communication was selected from the 4-bit CQI table defined in the 5G system [37]. Table 3 presents the CQI table [37] and the SINR regions required to achieve the target BLER. The SINR regions where each MCS can achieve the pre-configured required BLER (= 0.1) were determined based on the results of the link-level simulation of the HD system. The link-level parameters remained consistent with those listed in Table 1, except for the delay spread, which was set to 50 ns, approximating the mean value of the delay spread calculated from the hall size and room height [34].

In this simulation, the powers of the UL, DL, and IUI signals at the BS and DL-UE were ideally measured and reported in every slot, enabling the user scheduling and adaptive modulation algorithms to use the most up-to-date information. Additionally, considering the result of Figs. 8 and 9, both the threshold ρ and the amount of the IUIC C_{IUI}, which play a critical role in user scheduling and adaptive modulation algorithms, were set to -35 dB.

B. EFFECT OF TRANSMITTING POWER OF BS AND UE

Fig. 10(a) shows the ratio of the average user throughput of the 5G-DDC system with and without the proposed IUIC to that of the HD system. Fig. 10(b) shows the ratio of the 5% user throughput. Additionally, the IBFD application ratios in the UL and DL slots, both with and without IUIC, are illustrated in Fig. 10(c). The horizontal axis represents P_0, which relates to the transmission (Tx) power of the UE, as described in (11). The right end of the horizontal axis represents the scenario where the Tx power of the UE is fixed at the maximum power.

Regardless of the IUIC usage, an increase in P_0 (i.e., higher Tx power of the UE) leads to a gain in DL average throughput and 5% throughput, with both converging to approximately 165% and 142%, respectively. However, the performance with the proposed IUIC is slightly inferior to that without IUIC because the IBFD application ratio in the UL slot exhibits minimal changes, as shown in Fig. 10(c), while IUIC has a marginally negative impact on the success ratio of DL communication.

In the range of -100 dB $\leq P_0 \leq -90$ dB, as P_0 increases, the gains of the UL average and 5% throughput become significant primarily because the MCSs for the UL communication in both the UL and DL slots improve with higher UE Tx power.

However, in the range of -85 dB $\leq P_0$, the gains of the UL average and 5% throughput decrease as P_0 increases owing to the increasing IUI power and a reduction in the IBFD application ratio in the DL slot. Nevertheless, the IUIC can mitigate this reduction in gain when the Tx power of the UE is adequately high. As shown in Fig. 10(c), the IUIC increases the IBFD application ratio in the DL slot from 9.8% to 60.8% when the Tx power of the UE is at its maximum. Consequently, because of the increased opportunity for UL communications, the gains in the UL average and 5% throughput increase from 109.6% to 121.0% and 100.6% to 106.6%, as shown in Fig. 10(a) and (b), respectively.

IUIC can improve the IBFD application ratio in the DL slot but not in the UL slot so much. As described in Section III-D, in the DL slot, the UL-UE can adjust the MCS for UL communication based on the IUI power at the DL-UE.

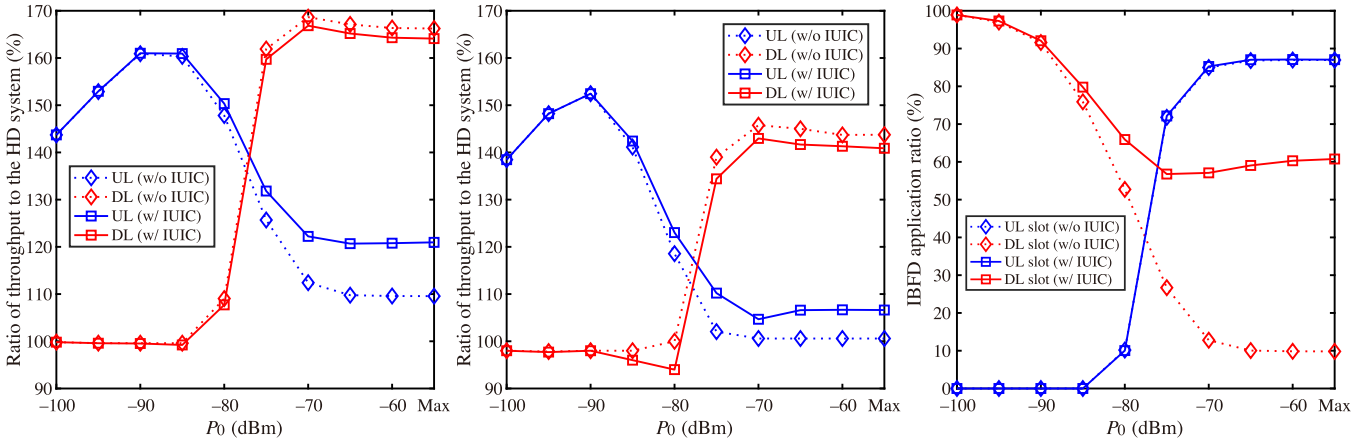

(a) Average user throughput (b) 5% user throughput (c) IBFD application ratio

FIGURE 10. Performance of the 5G-DDC system as a function of P_0 when the Tx power of BS is 27 dBm.

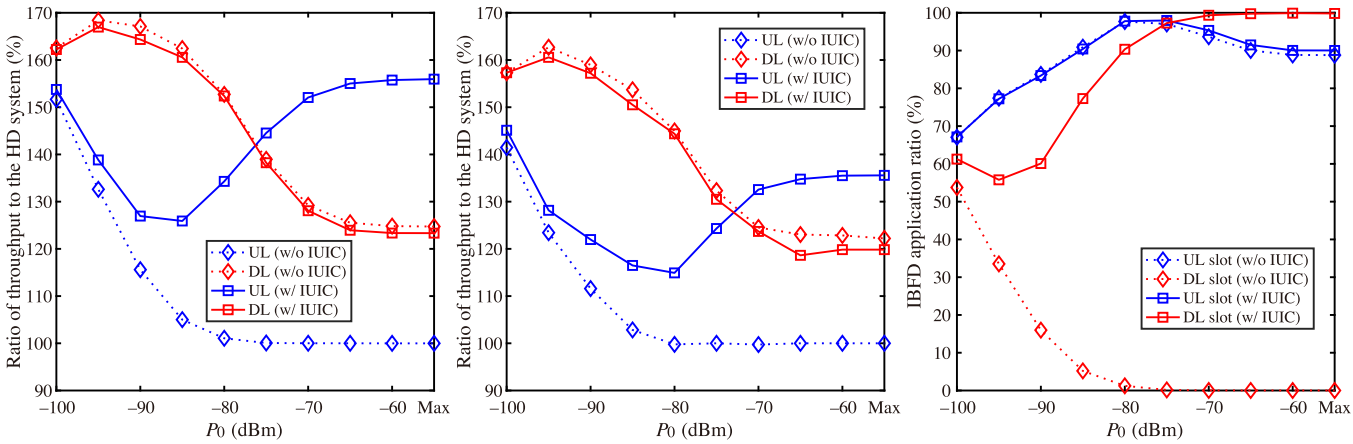

(a) Average user throughput (b) 5% user throughput (c) IBFD application ratio

FIGURE 11. Performance of the 5G-DDC system as a function of P_0 when the Tx power of BS is 10 dBm.

This enables the DL-UE to demodulate the UL signal (i.e., the IUI signal) during the IUIC process. Essentially, the available position of the DL-UE relative to the UL-UE can be adjusted by changing the MCS for the superimposed UL communication. Therefore, the number of UL-UE candidates in the DL slot with IUIC increases. However, in the UL slot, the MCS for the UL communication is predetermined. Hence, the IUIC cannot significantly increase the number of DL-UE candidates in the UL slot because the relative position of the DL-UE that can effectively use IUIC is limited by the fixed UL MCS.

The power constraints and interference considerations are crucial in real-world operations to avoid interference with other systems, such as adjacent cellular and public 5G systems. Under these circumstances, the impact of IUI can become more significant, affecting IBFD application and overall system performance.

Fig. 11 shows the ratio of throughput to the HD system and IBFD application when the Tx power of the BS is fixed at 10 dBm. The trends in Fig. 11 are similar to those shown in Fig. 10, where the Tx power of the BS was set to 27 dBm. However, the gains in the UL average and 5% throughput in Fig. 11(a) and (b) are larger than those in Fig. 10(a) and (b), respectively. In particular, the gains in the UL average and 5% throughput increase from 99.99% to 156.0% and from 100.0% to 135.6%, respectively, when the Tx power of the UE is maximum. The IBFD application ratio in the DL slot rapidly decreases and converges to 0% without using IUIC with increasing P_0 because the impact of IUI is relatively more significant. However, with IUIC, in the range of -95 dB $\leq P_0$, the application of IBFD increases and converges to 99.8% as P_0 increases. Therefore, the gains in UL communication increases.

C. EFFECT OF THE NUMBER OF UE

The number of UE in a system can significantly impact its performance. Figs. 12 and 13 illustrate the throughput ratio to the HD system and IBFD application ratio as a function of the number of UEs. The Tx powers of the BS in Figs. 12 and 13 were set to 27 and 10 dBm, respectively. P_0 was set to -70 dBm because the gains of the user throughput and

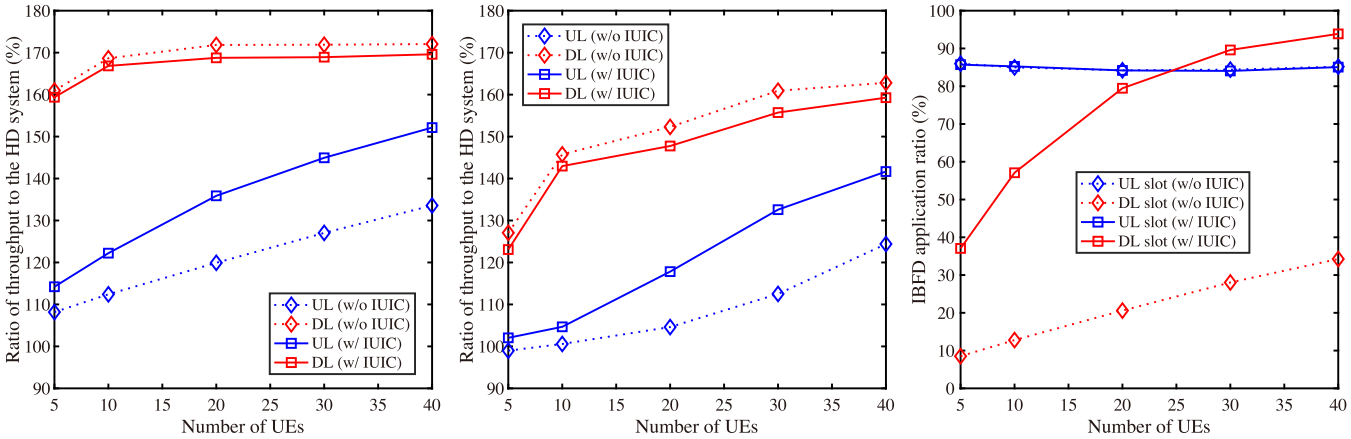

(a) Average user throughput (b) 5% user throughput (c) IBFD application ratio

FIGURE 12. Performance of the 5G-DDC system as a function of the number of UEs when the Tx power of BS is 27 dBm.

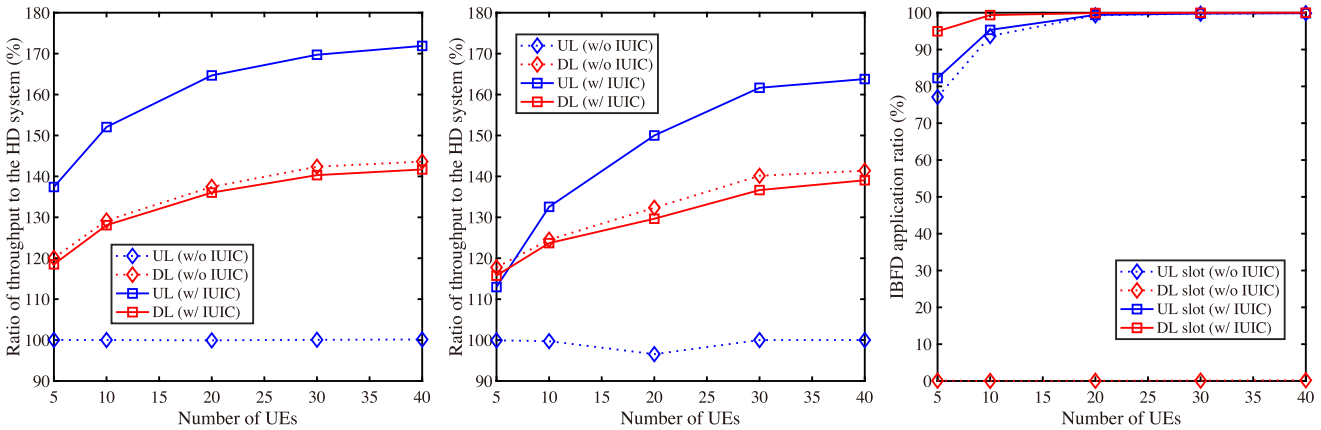

(a) Average user throughput (b) 5% user throughput (c) IBFD application ratio

FIGURE 13. Performance of the 5G-DDC system as a function of the number of UEs when the Tx power of BS is 10 dBm.

IBFD application ratio approximately converged, as shown in Figs. 10 and 11.

When the Tx power of the BS is 27 dBm, the gain of the average and 5% throughput increases with the number of UE. The signal with a higher MCS can be superimposed, increasing the gain, owing to increasing the number of candidates for DL-UE/UL-UE in the UL/DL slot. However, as the number of UE increases, the gain in the UL throughput with the IUIC becomes larger than that without the IUIC. This is attributed to a higher number of candidates for UL-UE intending to use the IUIC, increasing the IBFD application ratio in the DL slot, as shown in Fig. 12(c). However, the gain in DL throughput with the IUIC is approximately equivalent to that without the IUIC or slightly worse because the IUIC has limited ability to improve the IBFD application ratio in the UL slot, as discussed in Section V-B.

When the Tx power of the BS is 10 dBm, the improvement in the gain of the UL throughput with the IUIC is remarkable. Without IUIC, the gains in UL throughput are approximately 100%, regardless of the number of UEs, because the IBFD application ratio in the DL slot is approximately 0% owing to the high impact of IUI. However, the IBFD application ratio in the DL slot significantly increases with introducing the IUIC, reaching approximately 100% for ten or more UEs. Consequently, with 40 UEs, the gains of the UL average and 5% throughput increase from 100.1% to 171.9% and from 100.0% to 163.8%, respectively. Therefore, in scenarios with a low Tx power of the BS and the impact of the IUI is larger, the proposed IUIC is highly effective in improving the UL throughput.

D. EFFECT OF SI CANCELLATION PERFORMANCE

In the above evaluations, the SI cancellation performance was set to 110 dB, following the previous studies on DDC systems [21], [22]. However, when the Tx power of the BS was 27 dBm, the interference-to-noise power ratio (INR) after SI cancellation became 8 dB owing to the −91 dBm noise floor of BS. This value may decrease the system-level

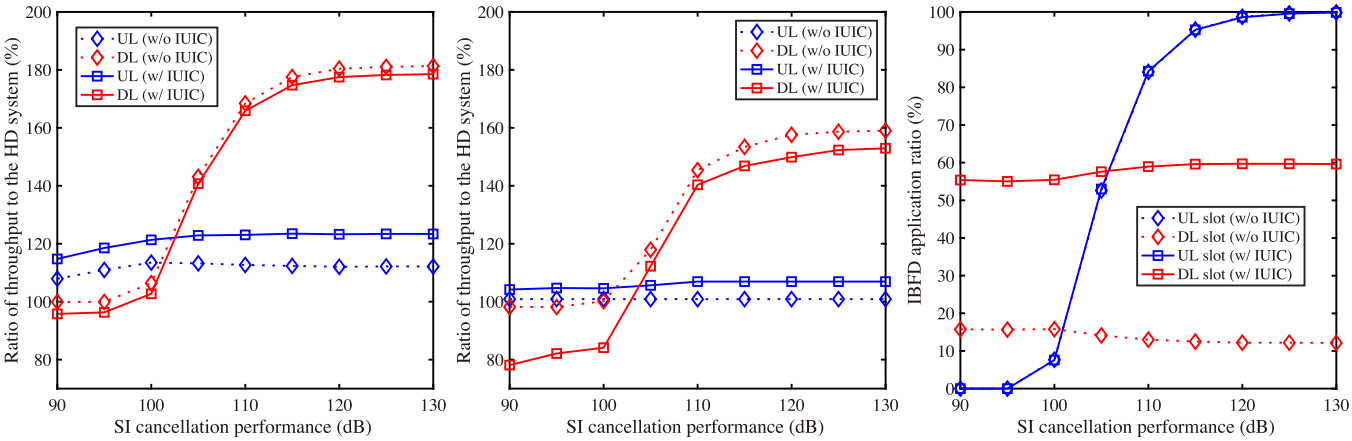

(a) Average user throughput (b) 5% user throughput (c) IBFD application ratio

FIGURE 14. Performance of the 5G-DDC system as a function of the SI cancellation performance when the Tx power of the BS is 27 dBm.

performance including the IUIC owing to the residual SI component. Therefore, this section evaluates the effect of the SI cancellation performance. Fig. 14 illustrates the throughput ratio to the HD system and IBFD application ratio as a function of the SI cancellation performance when the Tx power of BS and P_0 are set to 27 dBm and −70 dBm, respectively.

As shown in Fig. 14(c), the IBFD application ratio in the UL slot increases with an increase in the SI cancellation performance, regardless of the use of the IUIC. This is because the original UL communication is not interfered with the residual SI component, and the number of DL-UE candidates that satisfy the first condition in (9) increases. When the SI cancellation performances are 110 dB and 130 dB, the IBFD application ratios in the UL slot with the IUIC are 84.3% and 99.9%, respectively. On the other hand, little variation is observed in the IBFD application ratio in the DL slot. If the SI cancellation performance is increased from 110 dB to 130 dB, the IBFD application ratio in the DL slot remains almost the same. Additionally, regardless of the amount of SI cancellation, the proposed IUIC can improve the IBFD application ratio in the DL slot.

Consequently, the DL average and 5% throughput are greatly affected by the SI cancellation performance, as shown in Fig. 14(a) and (b). As the IBFD application ratio in the UL slot increases with the SI cancellation performance, the DL communication opportunities and gain of throughput increase and converge. However, a larger SI cancellation performance greater than 110 dB can improve DL throughput but has minimal impact on the effectiveness of the IUIC and UL throughput.

E. EFFECT OF TX POWER OF BS

In Figs. 10–13, the Tx power of the BS was set to 27 dBm or 10 dBm to change the relative strength of the IUI. However, it is important to perform a detailed evaluation of the effect of the Tx power of the BS. Therefore, this section evaluates the effect of the Tx power of the BS on the IUIC and 5G-DDC. Fig. 15 illustrates the throughput ratio to the HD system and IBFD application ratio as a function of the Tx power of the BS when the SI cancellation performance and P_0 are 110 dB and −70 dBm, respectively.

As shown in Fig. 15(c), in the UL slot, regardless of the use of the IUIC, as the Tx power of the BS increases, the IBFD application ratio increases when the Tx power of the BS is between 0 dBm and 15 dBm. This is because the larger Tx power of the BS diminishes the impact of IUI. However, as the Tx power of the BS increases from 15 dBm, the IBFD application ratio decreases under the crucial effect of SI with 110 dB SI cancellation. On the other hand, in the DL slot, the IBFD application ratio without the IUIC increases with the Tx power of the BS. This is because the effect of IUI is smaller. However, the IBFD application ratio is low owing to the IUI. The IUIC can increase the IBFD application ratio in the DL slot, especially assuming the low Tx power of the BS. The IBFD application ratio decreases with an increase in the Tx power of the BS because the power difference between the IUI and desired signal becomes small, making it difficult to utilize the IUIC.

According to these characteristics of the IBFD application ratios, the gains of the average and 5% throughput changes, as shown in Fig. 15(a) and (b). Regardless of the use of the IUIC, the gains of the DL throughputs increase with the Tx power of the BS. However, when the Tx power of the BS is 27 dBm, they decrease because of SI. As described in Section V-B, the IUIC is more effective on the UL average and 5% throughput. The smaller the Tx power, the greater the effectiveness of the IUIC. In particular, when the Tx power of the BS is 0 dBm, the gains of the UL average and 5% throughput increase from 100.0% to 176.0% and 99.6% to 160.0%, respectively. Therefore, because the Tx power of the BS affects the system-level performance, various parameters, such as the SI cancellation performance and the Tx power of the BS and UE, should be appropriately designed according to the desired performance.

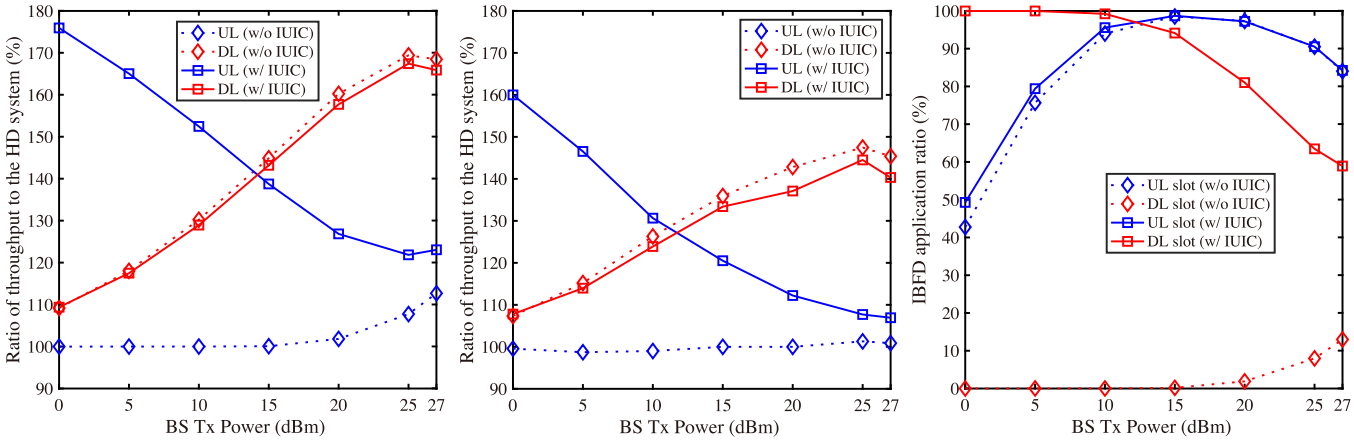

(a) Average user throughput (b) 5% user throughput (c) IBFD application ratio

FIGURE 15. Performance of the 5G-DDC system as a function of the Tx power of the BS when the SI cancellation performance is 110 dB.

VI. FUTURE WORKS

This study aimed to introduce the IBFD with the IUIC into a 5G system. However, its applicability and effectiveness must be further evaluated from following the four viewpoints to implement the proposed system in society, and new schemes for the IUIC should be proposed in the future if necessary.

The first is the user density or the number of UEs. This thesis evaluated the effect of the number of UEs on the user throughput, but the larger number of UEs causes a further larger system overhead to collect IUI information. Considering the overhead, the gain of the user throughput may not be obtained even with the IBFD. Therefore, the effectiveness of the proposed system should be evaluated, including the impact of the system overhead.

The second is the various mobility scenarios. We introduced IBFD into the local 5G, such as an indoor factory environment, with low mobility. The signal processing of the IUIC is expected to work in an environment with higher mobility, but the old IUI information will affect the proposed scheduling and adaptive modulation algorithms. Therefore, it is essential to evaluate the impact of the mobile speed along with the proposal of a new protocol.

The third is the deployment scenarios. When the IBFD is introduced into not a single-cell but a multi-cell environment, the effect of ICI will affect the scheduling and adaptive modulation algorithms. The ICI decreases the system-level performance, even in the conventional DDC and FDC systems. Although the proposed IUIC does not at least increase the impact of ICI, the evaluation of the various deployment scenarios will provide insights for new IUIC schemes and scheduling algorithms in the future.

The fourth is the number of antennas. In this study, a SISO environment was assumed, where the SIC-based IUIC may be the most effective because other schemes, such as beamforming [15] and nulling signal forwarding [16], should use multiple antennas. However, combining the IBFD with MIMO will be necessary to further enhance spectral efficiency in some scenarios. Therefore, we should expand the proposed schemes to adapt to MIMO and compare their effectiveness with other IUIC schemes in the future.

As generating signals for transmitting user data (i.e., PDSCH, PUSCH, and DMRS) follows the 5G standard, the demodulation characteristics conform to it. However, this study did not consider exchanging the control signal, such as downlink control information (DCI) and uplink control information (UCI). Furthermore, this study assumed the ideal measurement and feedback of the IUI information. These assumptions may give our IUIC schemes resilience to the mobility and number of accommodated terminals, as mentioned above. Therefore, control and feedback protocols for the IUI information should be proposed in the future.

VII. CONCLUSION

This study proposed an IUIC scheme using SIC based on a 5G signal format to improve the performance of 5G-FDC and 5G-DDC. The IUIC approach includes methods for LLR calculation to improve demodulation and cancellation performance and a decision-making process to determine when to use the IUIC. Additionally, user scheduling and adaptive modulation algorithms were introduced for operating a 5G-based DDC system. We evaluated the effectiveness of the IUIC through link- and system-level simulations. The link-level simulation showed that the DL-UE could demodulate the desired signal with a 3.4 dB deterioration compared to the HD system, even when SIR was −40 dB. The system-level simulation showed that IUIC could significantly improve the IBFD application ratio in the DL slot and the user throughput of UL communication. In cases where the Tx powers of the BS and UE were maximum, IUIC increased the IBFD application ratio in the DL slot from 9.8% to 60.8%. Moreover, it led to gains of 109.6% to 121.0% and 100.6% to 106.6% in the UL average and 5% throughput, respectively, with a slight deterioration in the user throughput of DL communication. This reduction occurred because IUIC had a slightly adverse impact on the reception quality of DL communication, even though it improved the IBFD application ratio in the UL slot.

The effectiveness of the IUIC was increased with a decrease in the Tx power of the BS or an increase in the number of UEs. In particular, when the Tx power of BS and the number of UEs were 10 dBm and 40, respectively, the IBFD application ratio in the DL slot increased from 0.2% to 100%. The gains of the UL average and 5% throughput increased from 100.1% to 171.9% and from 100.0% to 163.8%, respectively. Future research efforts may focus on further refining the digital signal processing of the IUIC, user scheduling, and adaptive modulation algorithms, to further enhance UL throughput and DL throughput.

REFERENCES

[1] A. Ghosh, A. Maeder, M. Baker, and D. Chandramouli, "5G evolution: A view on 5G cellular technology beyond 3GPP release 15," *IEEE Access*, vol. 7, pp. 127639–127651, 2019.

[2] Samsung, "6G the next hyper—Connected experience for all.," White paper, Jul. 2020.

[3] D. Kawamatsu, K. Mizutani, and H. Harada, "Highly efficient relay routing method for 5G cellular V2V communications," in *Proc. IEEE Conf. Standards Commun. Netw.*, 2022, pp. 218–223.

[4] S. Han et al., "Artificial-intelligence-enabled air interface for 6G: Solutions, challenges, and standardization impacts," *IEEE Commun. Mag.*, vol. 58, no. 10, pp. 73–79, Oct. 2020.

[5] X. Han et al., "Interference mitigation for non-overlapping sub-band full duplex for 5G-Advanced wireless networks," *IEEE Access*, vol. 10, pp. 134512–134524, 2022.

[6] X. Lin, "An overview of 5G advanced evolution in 3GPP release 18," *IEEE Commun. Standards Mag.*, vol. 6, no. 3, pp. 77–83, Sep. 2022.

[7] W. Chen, J. Montojo, J. Lee, M. Shafi, and Y. Kim, "The standardization of 5G-advanced in 3GPP," *IEEE Commun. Mag.*, vol. 60, no. 11, pp. 98–104, Nov. 2022.

[8] Nokia, "5G-advanced: Expanding 5G for the connected world," White paper, 2023.

[9] D. Kim, H. Lee, and D. Hong, "A survey of in-band full-duplex transmission: From the perspective of PHY and MAC layers," *IEEE Commun. Surveys Tuts.*, vol. 17, no. 4, pp. 2017–2046, Fourthquart. 2015.

[10] D. Bharadia et al., "Full duplex radios," in *Proc. ACM SIG-COMM*, 2013, pp. 375–386.

[11] E. Everett, A. Sahai, and A. Sabharwal, "Passive self-interference suppression for full-duplex infrastructure nodes," *IEEE Trans. Wireless Commun.*, vol. 13, no. 2, pp. 680–694, Feb. 2014.

[12] S. Mori, K. Mizutani, and H. Harada, "A digital self-interference cancellation scheme for in-band full-duplex-applied 5G system and its software-defined radio implementation," *IEEE Open J. Veh. Technol.*, vol. 4, pp. 444–456, 2023.

[13] M. S. Sim, M. Chung, D. Kim, J. Chung, D. K. Kim, and C.-B. Chae, "Nonlinear self-interference cancellation for full-duplex radios: From link-level and system-level performance perspectives," *IEEE Commun. Mag.*, vol. 55, no. 9, pp. 158–167, Sep. 2017.

[14] A. Sabharwal, P. Schniter, D. Guo, D. W. Bliss, S. Rangarajan, and R. Wichman, "In-band full-duplex wireless: Challenges and opportunities," *IEEE J. Sel. Areas Commun.*, vol. 32, no. 9, pp. 1637–1652, Sep. 2014.

[15] E. Aryafar and A. Keshavarz-Haddad, "FD^2: A directional full duplex communication system for indoor wireless networks," in *Proc. IEEE Conf. Comput. Commun.*, Aug. 2015, pp. 1993–2001.

[16] Y. Lee and B. -Y. Huang, "Active interference cancellation for full-duplex multiuser networks with or without existence of self-interference," *IEEE Access*, vol. 7, pp. 15056–15068, 2019.

[17] K. C. -J. Lin, K. -C. Hsu, and H. -Y. Wei, "Inter-client interference cancellation for full-duplex networks with half-duplex clients," *IEEE/ACM Trans. Netw.*, vol. 27, no. 5, pp. 2150–2163, Oct. 2019.

[18] W. Zhao, C. Feng, F. Liu, C. Guo, and Y. Nie, "Blind polarization oblique projection based inter-user interference cancellation in full duplex multiuser MIMO system," in *Proc. IEEE 28th Annu. Int. Symp. Pers., Indoor, Mobile Radio Commun.*, 2017, pp. 1–5.

[19] M. Liu, Y. Mao, S. Leng, and K. Yang, "Successive interference cancellation in full duplex cellular networks," in *Proc. IEEE Int. Conf. Commun.*, 2017, pp. 1–6.

[20] S. Mori, K. Mizutani, and H. Harada, "In-band full-duplex-applicable area expansion by inter-user interference reduction using successive interference cancellation," *IEICE Trans. Commun.*, vol. E105-B, no. 2, pp. 168–176, Feb. 2022.

[21] K. Nishikori, K. Teramae, K. Mizutani, T. Matsumura, and H. Harada, "User throughput enhancement with dynamic full-duplex cellular system in dense urban multi-cell environment," in *Proc. IEEE 30th Annu. Int. Symp. Pers., Indoor Mobile Radio Commun.*, 2019, pp. 1–6.

[22] K. Fukushima, S. Mori, K. Mizutani, and H. Harada, "Throughput enhancement of dynamic full-duplex cellular system by distributing base station reception function," *IEEE Open J. Veh. Technol.*, vol. 4, pp. 114–126, 2023.

[23] S. Goyal et al., "Full duplex cellular systems: Will doubling interference prevent doubling capacity?," *IEEE Commun. Mag.*, vol. 53, no. 5, pp. 121–127, May 2015.

[24] A. Tang and X. Wang, "A-duplex: Medium access control for efficient coexistence between full-duplex and half-duplex communications," *IEEE Trans. Wireless Commun.*, vol. 14, no. 10, pp. 5871–5885, Oct. 2015.

[25] W. Choi, H. Lim, and A. Sabharwal, "Power-controlled medium access control protocol for full-duplex WiFi networks," *IEEE Trans. Wireless Commun.*, vol. 14, no. 7, pp. 3601–3613, Jul. 2015.

[26] G. C. Alexandropoulos, M. Kountouris, and I. Atzeni, "User scheduling and optimal power allocation for full-duplex cellular networks," in *Proc. IEEE 17th Int. Workshop Signal Process. Adv. Wireless Commun.*, 2016, pp. 1–6.

[27] R. Kiran and N. B. Mehta, "User-pair scheduling and mode selection in asymmetric full-duplex systems with limited feedback: Algorithm and scaling laws," *IEEE Trans. Wireless Commun.*, vol. 20, no. 5, pp. 2863–2875, May 2021.

[28] R. Kwan, C. Leung, and J. Zhang, "Proportional fair multiuser scheduling in LTE," *IEEE Signal Process. Lett.*, vol. 16, no. 6, pp. 461–464, Jun. 2009.

[29] H. Yin, L. Zhang, and S. Roy, "Multiplexing URLLC traffic within eMBB services in 5G NR: Fair scheduling," *IEEE Trans. Commun.*, vol. 69, no. 2, pp. 1080–1093, Feb. 2021.

[30] 3GPP, "Physical layer procedures for control," 3GPP, Sophia Antipolis, France, Tech. Specification 38.213 V17.7.0, Sep. 2023.

[31] 3GPP, "Physical channels and modulation," 3GPP, Sophia Antipolis, France, Tech. Specification 38.211 V17.6.0, Sep. 2023.

[32] 3GPP, "Multiplexing and channel coding," 3GPP, Sophia Antipolis, France, Tech. Specification 38.212 V17.6.0, Sep. 2023.

[33] S. Schwandter, P. Fertl, C. Novak, and G. Matz, "Log-likelihood ratio clipping in MIMO-BICM systems: Information geometric analysis and impact on system capacity," in *Proc. IEEE Int. Conf. Acoust., Speech Signal Process.*, 2009, pp. 2433–2436.

[34] 3GPP, "Study on channel model for frequencies from 0.5 to 100 GHz," 3GPP, Sophia Antipolis, France, Tech. Rep. 38.901 V17.0.0, Mar. 2022.

[35] 3GPP, "Study on physical layer enhancements for NR ultra-reliable and low latency case (URLLC)," 3GPP, Sophia Antipolis, France, Tech. Rep. 38.824 V16.0.0, Mar. 2019.

[36] 3GPP, "Study on evolution of NR duplex operation," 3GPP, Sophia Antipolis, France, Tech. Rep. 38.858 V1.0.0, Sep. 2023.

[37] 3GPP, "Physical layer procedures for data," 3GPP, Sophia Antipolis, France, Tech. Specification 38.214 V17.7.0, Sep. 2023.

SHOTA MORI (Member, IEEE) received the B.E. degree from the Faculty of Engineering, Kyoto University, Kyoto, Japan, in 2021, and the M.I. and Ph.D. degrees from the Graduate School of Informatics, Kyoto University, in 2023 and 2024, respectively. He is currently a Research Fellow PD with Kyoto University with the Japan Society for the Promotion of Science. His research interests include physical layer technologies of 6th generation mobile communication (6G) system. He was the recipient of the Student Paper Award from IEEE VTS Tokyo/Japan Chapter in 2021 and Student Award from IEICE technical committee on SRW in 2022.

KEIICHI MIZUTANI (Member, IEEE) received the B.E. degree in engineering from Osaka Prefecture University, Sakai, Japan, in 2007, and the M.E. and Ph.D. degrees in engineering from the Tokyo Institute of Technology, Tokyo, Japan, in 2009 and 2012, respectively. He is currently an Associate Professor with the Graduate School of Informatics, Kyoto University, Kyoto, Japan. He was an Invited Researcher with Fraunhofer Heinrich Hertz Institute, Berlin, Germany, in 2010. From 2012 to 2014, he was a Researcher with the National Institute of Information and Communications Technology (NICT), Tokyo, Japan. From 2014 to 2021, he was an Assistant Professor with the Graduate School of Informatics, Kyoto University. From 2021 to 2022, he was an Associate Professor with the School of Platforms, Kyoto University. His research interests include physical layer technologies in white space communications, dynamic spectrum access, wireless smart utility networks (Wi-SUN), and 4G/5G/6G systems, OFDM, OFDMA, MIMO, multihop relay network, and full-duplex cellular systems. Since joining NICT, he has been involved in IEEE 802 standardization activities, namely 802.11af, 802.15.4m, and 802.22b. He was the recipient of the Special Technical Awards from IEICE SR technical committee in 2009 and 2017, Best Paper Award from IEICE SR technical committee in 2010 and 2020, Young Researcher's Award from IEICE SRW technical committee in 2016, Best Paper Award from WPMC2017 and WPMC2020, and Best Paper Presentation Award (1st Place) from IEEE WF-IoT 2020.

HIROSHI HARADA (Senior Member, IEEE) is currently a Professor with the Graduate School of Informatics, Kyoto University, Kyoto, Japan, and an Executive Research Director of Wireless Networks Research Center, National Institute of Information and Communications Technology (NICT), Tokyo, Japan. In 1995, he joined the Communications Research Laboratory, Ministry of Posts and Communications (currently, NICT). He has authored the book entitled *Simulation and Software Radio for Mobile Communications* (Artech House, 2002). Since 1995, he has researched software radio, cognitive radio, dynamic spectrum access network, wireless smart ubiquitous network (Wi-SUN), and broadband wireless access systems. He also has joined many standardization committees and forums in the United States as well as in Japan and fulfilled important roles for them, especially IEEE 1900 and IEEE 802. He was the Chair of IEEE DySpan Standards Committee and a Vice Chair of IEEE 802.15.4g, IEEE 802.15.4m, IEEE 1900.4, and TIA TR-51. He was a Board of Directors of IEEE Communication Society Standards Board, SDR forum, DSA alliance, and WhiteSpace alliance. He is a Cofounder of Wi-SUN alliance and was the Chairman of the board from 2012 to 2019. He is a Vice Chair of IEEE 2857, IEEE 802.15.4aa, and Wi-SUN alliance. He was the Chair of the IEICE Technical Committee on Software Radio (TCSR) and Chair of Public Broadband Mobile Communication Development Committee, ARIB. He is also involved in many other activities related to telecommunications. He was the recipient of the achievement awards in 2006 and 2018 and fellow of IEICE in 2009, respectively and the achievement awards of ARIB in 2009 and 2018, respectively, on the topic of research and development on software radio, cognitive radio, and Wi-SUN.